



# Effects of clamping design on the ballistic impact response of soft body armor

Gaurav Nilakantan<sup>1</sup>, Steven Nutt<sup>1,\*</sup>

1. Mork Family Department of Chemical Engineering and Materials Science, M.C. Gill Composites Center, University of Southern California, Los Angeles, CA 90089, USA.

**Abstract:** The effects of clamping on the ballistic impact performance of non-backed woven aramid fabrics is studied by considering several clamping configurations including 4-sided, 2-sided, circular, diamond, and corner-clamped frames.  $V_{50}$  velocities were estimated through several deterministic finite element impact simulations at varying impact velocities. Impacts occurring both directly on a yarn and the inter-yarn gap were considered. The different clamping configurations resulted in different fabric deformation, failure, and energy dissipating mechanisms. The circular frame resulted in the highest fabric  $V_{50}$  velocity. The  $V_{50}$  velocities were often sensitive to the precise projectile impact location relative to the principal yarns. Impact tests with fabrics clamped using four corner plates showed tearing at the corners. Fabrics clamped at their four corner points showed distinct deformation and failure mechanisms over three impact velocity regimes.

Key words: Fabrics, Ballistic impact, Finite element analysis,  $V_{50}$  velocity.

## 1. Introduction

Soft body armor used by military and law enforcement often consists of aramid materials (e.g., Kevlar) in the form of multiple layers of stitched plain-weave fabric. More information on these

Please cite this article as: Nilakantan G, Nutt S. *Effects of clamping design on the ballistic impact response of soft body armor*. Composite Structures 108 (2014) 137–150. DOI: <http://dx.doi.org/10.1016/j.compstruct.2013.09.017>



materials used for soft body armor, their experimental characterization, and numerical modeling under ballistic impact can be obtained from Refs. [1–5]. The ballistic impact performance of soft body armor is characterized through probabilistic velocity parameters such as the V0 and V50 velocities. VX velocity refers to the impacting projectile or threat velocity that has an X% probability of fully penetrating through the armor target. The probabilistic nature of armor penetration arises from several sources of statistical variability that may be intrinsic to the fabric-based armor system, such as filament and yarn geometrical and material properties (e.g., statistical tensile strength, frictional interactions, filament cross-section, filament packing) or extrinsic to the armor system, which are often related to the experimental testing methods (e.g., precise impact location, fabric slippage from clamps). These factors have been extensively studied by Nilakantan et al. [6–12]. While the V50 velocity is obtained through destructive experimental testing over a range of impact velocities, Nilakantan et al. [6,7] have developed computational techniques to numerically predict the entire probabilistic impact behavior of a woven fabric target. This behavior is represented through the probabilistic velocity response (PVR) curve, or V0–V100 curve. The computational technique maps the different sources of statistical variability into the finite element model. Computational studies have important advantages over experimental impact studies, perhaps the most notable being the ability to eliminate unwanted sources of variability and error that bias the probabilistic impact response, and the ability to carefully control and reproduce the test parameters that constitute the impact scenario. Other important advantages include the ability to study the isolated and coupled effects of multiple sources of variability by controlling the input to the finite element model, being able to isolate the individual components of overall energy dissipation, and track the deformation and failure of individual yarns. Experimentally, it is extremely difficult to

obtain resolution at a yarn-level or to observe in detail the complex mechanisms and interactions

Please cite this article as: Nilakantan G, Nutt S. *Effects of clamping design on the ballistic impact response of soft body armor*. Composite Structures 108 (2014) 137–150. DOI:

<http://dx.doi.org/10.1016/j.compstruct.2013.09.017>



that occur at the impact site. Obviously, the greater the field of view during the experimental impact test, the poorer is the resolution of recorded data or images. An important limitation of computational studies is the size of a fabric target modelled at a yarn-level that can be run within a reasonable amount of time using available computational infrastructure. Often these simulated finite element models are nowhere near the size of the actual armor application. However, multiscale fabric models based on hybrid element analysis developed by Nilakantan et al. [13,14] have begun to address the imbalance between degree of modeling resolution and size of the fabric model, thereby providing a path forward to scale up the size of fabric models.

Broadly, the ballistic impact testing of woven fabric targets can be divided into backed and non-backed testing. The former employs a backing material such as ballistic gel or clay (e.g., Roma plastilina) placed directly behind the fabric target. The clay is used to represent the human torso. The latter uses fixture plates and clamps to hold the fabric in different configurations, and no backing material is used. While clay-backed fabric targets appear to provide a more realistic representation of the behavior of soft body armor under small arms fire, there are important limitations to consider. Firstly, the clay itself constitutes a source of variability that affects the PVR curve. Secondly, the amount of recordable data, especially instantaneously during the test, is limited by the presence of the clay, precluding the use of high-speed photography. Non-backed clamped and unclamped fabric targets provide more useful information during an experimental test, and based on the clamping configuration, the dominant mechanisms of energy dissipation and failure can be manipulated, thereby providing useful insight on how to tailor the ballistic impact performance. However, an important limitation of using clamped fabrics is the boundary slippage that can occur during impact, and unfortunately, this has not been given much attention in the literature. Nilakantan et al. [15,16]

showed that this slippage, even very small extents, can dramatically affect the probabilistic impact response of soft body armor. Please cite this article as: Nilakantan G, Nutt S. *Effects of clamping design on the ballistic impact response of soft body armor*. Composite Structures 108 (2014) 137–150. DOI: <http://dx.doi.org/10.1016/j.compstruct.2013.09.017>



performance. Consequently, fabric slippage is an undesirable extrinsic source of variability. It also makes comparisons with numerical predictions difficult, because numerical fabric models often model perfectly clamped or zero-slippage boundaries. There have been several experimental impact studies on non-backed and clamped single aramid yarns and woven fabric targets that have attempted to measure yarn and fabric strains and projectile residual velocities using embedded wires, digital image correlation, high speed photography, and light/magnetic screens [15,17–20].

Different researchers have used different clamping configurations when shooting fabric targets, such as 4-sided frames and circular clamps, and it is not well understood how the shapes of these clamps precisely affect the mechanisms of deformation and energy dissipation in the fabric, and consequently the impact performance. The most commonly used ballistic impact performance metric is the  $V_{50}$  velocity, which is usually normalized by the fabric areal density. However in this study, we demonstrate how the clamping design itself affects the  $V_{50}$  velocity prediction for a constant exposed fabric area and projectile type. Obviously, this becomes an important consideration when comparing the ballistic impact performances of different fabric targets across different laboratories.

## **2. Methodology**

### **2.1 Material**

A single layer of plain weave aramid fabric (Kevlar S706) is used in this study. The areal density of the fabric is  $180 \text{ g/m}^2$  with an approximate thickness of 0.23 mm. The warp and fill yarns are 600 denier Kevlar KM2 yarns with a yarn span of 0.747 mm. Each yarn is comprised of 400



approximately circular filaments of diameter 12  $\mu\text{m}$  and density 1.44  $\text{g/cm}^3$ . The longitudinal yarn tensile modulus is 82.6 GPa with a tensile strength of 3.4 GPa.

## 2.2 Clamp design

Fig. 1 displays the six different clamping configurations considered, including 4-sides held, 2 sides held, circular clamp, diamond clamp, and corner clamp. The corner clamp configuration consists of a corner plate held and a corner point held setup wherein the fabric is either clamped using four plates at each corner or simply held at the four extreme corners of the fabric which approximately represents a totally unclamped, free-standing fabric. In all cases, the exposed area of the fabric is kept constant at 5806.44  $\text{mm}^2$ . For the 4-sides and 2-sides held case, this implies the dimensions of the exposed square fabric are 76.20 mm x 76.20 mm. The circular clamped fabric has a diameter of 85.98 mm, while the diagonals of the diamond clamped fabric are 107.76 mm. The diamond frame is essentially the 4-sided frame rotated by 45°. For the corner plate clamped fabric, each of the four plates have dimensions of 34.08 mm x 34.08 mm while the overall dimensions of the fabric are 102.23 mm x 102.23 mm. The dimensions of the exposed square fabric for the corner point clamped fabric are the same as the 4-sides held case, and the fabric is clamped over two yarn widths at each of the four extreme corners.

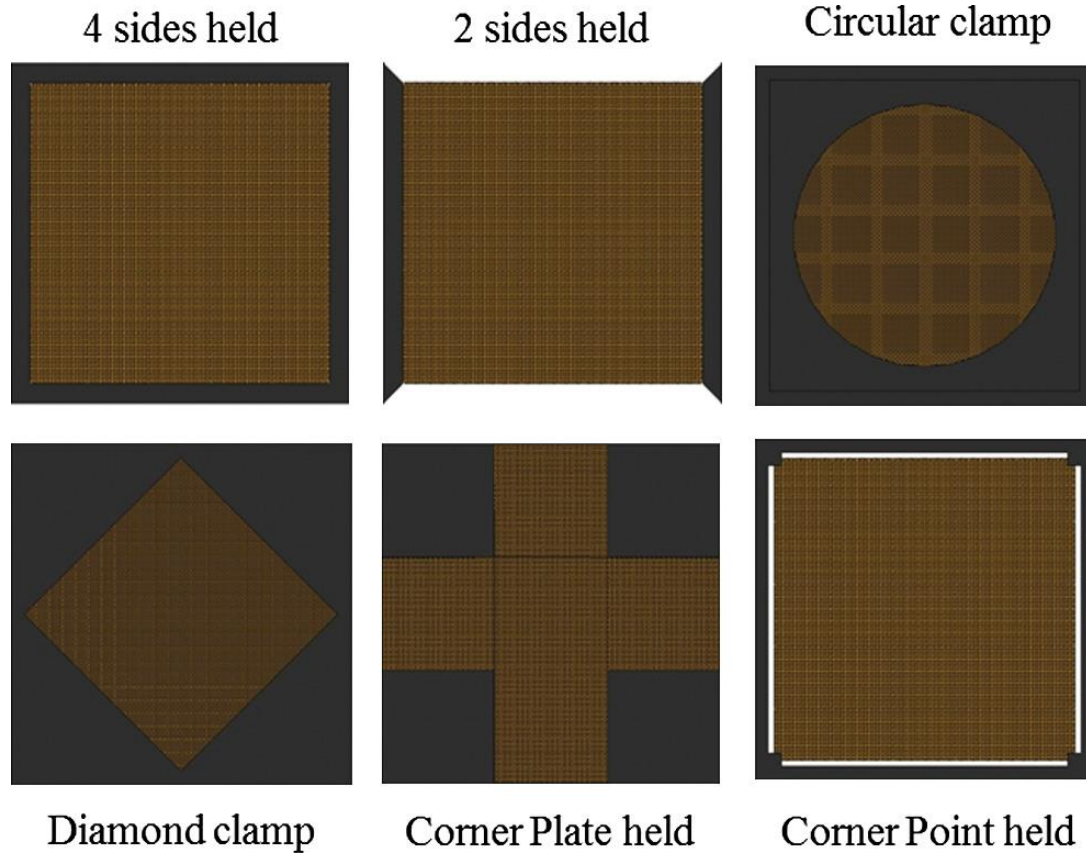


**Fig. 1.** Clamping configurations for the fabric impact testing.

### 2.3 Impact testing

For each of the clamping configurations with the exception of the corner clamps, a total of 16–18 test shots are conducted at varying impact velocities. For each velocity, impacts that occur exactly at a yarn cross-over (known as yarn impact) as well as the gap between two yarns (known as gap impact) are considered. A 0.22 caliber spherical steel projectile of mass 0.692 gm and diameter 5.556 mm impacts the single layer of fabric at its center. The outcome (penetration or non-penetration) is recorded along with the residual projectile velocity for penetrating impacts and peak fabric dynamic deflection for non-penetrating impacts. The energy dissipated ( $E_d$ ) by the fabric is given by

Please cite this article as: Nilakantan G, Nutt S. *Effects of clamping design on the ballistic impact response of soft body armor*. Composite Structures 108 (2014) 137–150. DOI: <http://dx.doi.org/10.1016/j.compstruct.2013.09.017>



$$E_d = \frac{1}{2} m_p (V_i^2 - V_r^2) \quad (1)$$

where  $m_p$  is the mass of the projectile,  $V_i$  is the impact velocity and  $V_r$  is the residual velocity. For non-penetrating impacts,  $V_r$  is assumed to be zero. Whenever a response jump is observed during testing, i.e. non-penetrating become penetrating impacts and vice versa, an impact velocity increment of 2.5 m/s is used. A 6-shot  $V_{50}$  velocity is then computed by calculating the average of the three highest non-penetrating and three lowest penetrating impact velocities. In addition, separate  $V_{50}$  velocities are computed for yarn-based impacts and gap-based impacts. These  $V_{50}$  velocities are computed by taking the average of the two velocities that bound the response jump, i.e., the highest non-penetrating shot and lowest penetrating shot velocity.

## 2.4 Finite element model

Individual Kevlar yarns are explicitly modeled as homogenous continua and are discretized with solid elements. The pre-processor DYNAFAB [21] is used to set up the fabric mesh. Both the warp and fill yarns are assumed to have the same degree of undulation or crimp. To account for the homogenization of the actual filament-level yarn architecture, the material properties must be adjusted by the filament volume fraction  $mf$ , which is computed as the ratio of the actual filament cross-sectional area to the cross-sectional area of the finite element yarn, resulting in a  $mf$  value of 87%. The yarns are assigned a transversely isotropic material model with the following adjusted properties:  $E_{axial}$  of 71.84 GPa ( $E_{11}$ ),  $E_{trans}$  of 718.45 MPa ( $E_{22}$ ,  $E_{33}$ ),  $G$  of 148 MPa ( $G_{12}$ ,  $G_{23}$ ,  $G_{31}$ ),  $\nu$  of 0.0 ( $\nu_{12}$ ,  $\nu_{23}$ ,  $\nu_{31}$ ), and  $\rho_{yarn}$  of 1.25 g/cm<sup>3</sup>. A coefficient of friction of 0.23 is used between the projectile and the fabric, and 0.18 between the warp and fill yarns. An element erosion-based failure model is used based on a maximum tensile stress failure criterion, with a  $r_{fail}$  of 2.95 GPa.





A zero slippage or perfectly clamped boundary condition is modeled by constraining all the degrees of freedom of the fabric nodes that are within the upper and lower clamps. The finite element code LS-DYNA [22] is used for all impact simulations.

### 3. Results and discussion

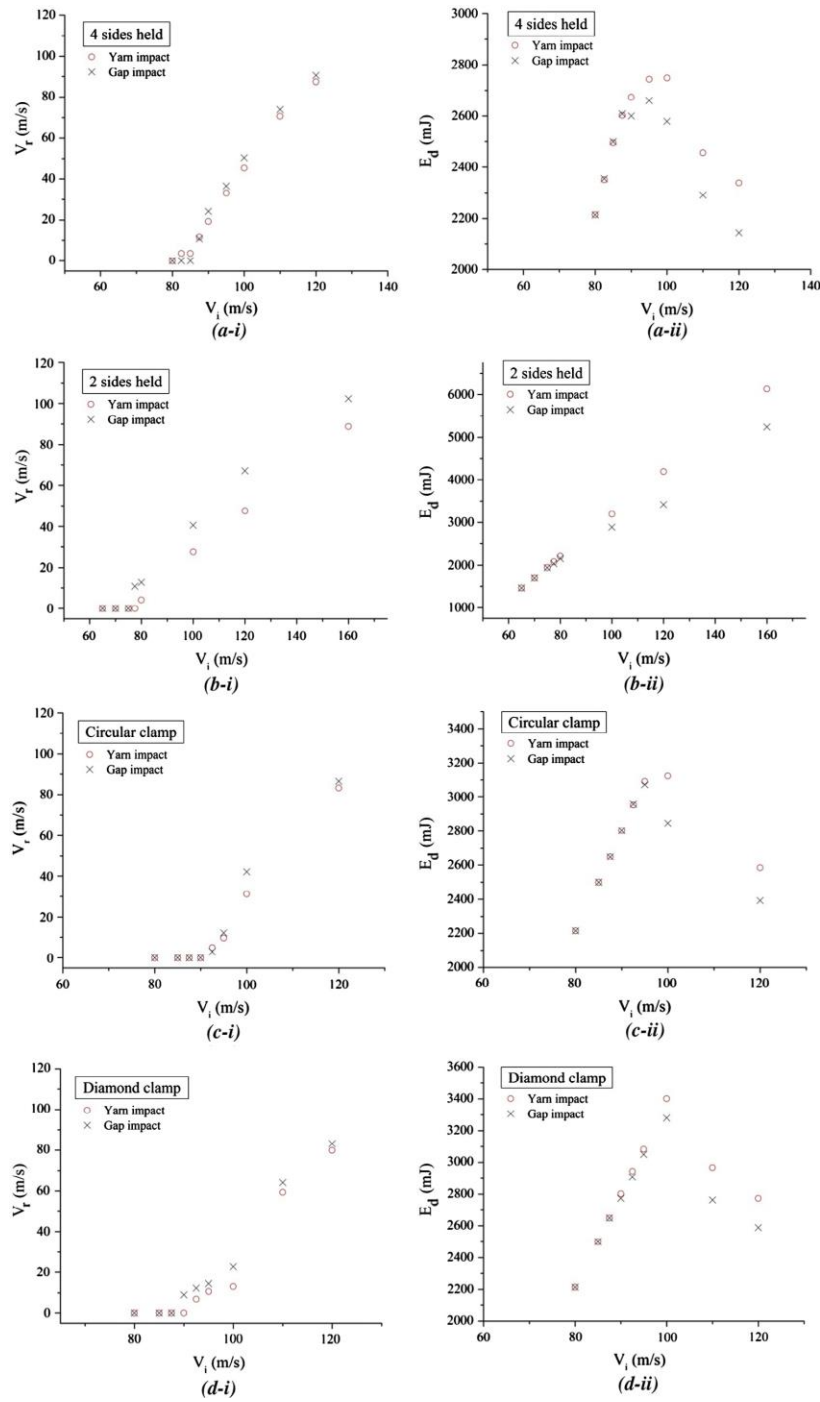
#### 3.1 4-Sided, 2-sided, circular, and diamond clamped fabrics

Fig. 2 displays  $V_i$ – $V_r$  plots and  $V_i$ – $E_d$  plots for all four clamp configurations. Test shots that represent yarn impacts are represented by ‘o’ while gap impacts are represented by ‘x’. All clamp configurations show sensitivity to the precise projectile impact location. The 2-sided case shows the most sensitivity at higher impact velocities. For the 2-sided case, the magnitude of energy dissipated by the fabric continually grows with increasing impact velocities, and the difference in magnitudes between the yarn impact- and gap impact-based energy dissipation continually grows also. This phenomenon is better understood by referring to Figs. 3 and 4. Fig. 3 displays the projectile velocity history for a 70 m/s impact of a 2-sided clamped fabric. The initial rate of deceleration is the same for both the yarn and gap impacts. The point of deviation in velocity histories occurs at  $\sim 215 \mu\text{s}$ , as denoted by the arrow in Fig. 3, which represents the time instant at which the transverse displacement wave has returned to the impact site after reflecting from the clamped edges. At this time instant, several warp yarns (which are clamped) at the impact site fail in tension, and the unclamped fill yarns start to pull out of the fabric weave. From this point on until the projectile is completely arrested, the gap impact shows a much faster rate of projectile deceleration, resulting in a faster projectile arrest. Fig. 4 displays the fabric deformation states at the time instant of zero residual





projectile velocity or complete projectile arrest. The gap impact has resulted in the central two fill yarns pulling out of the weave. In contrast, the yarn impact results in only the central-most fill yarn pulling out, while the adjacent fill yarns are pushed aside by the projectile. For a 2-sided clamped case, frictional energy dissipations due to yarn pullout is a major source of energy dissipation. Consequently, the pullout of two yarns simultaneously for the gap impact results in a greater rate of energy dissipation and a faster projectile deceleration.



**Fig. 2.** (i) Impact vs residual velocity plot (ii) impact velocity vs energy dissipated plot for (a) 4-sides held, (b) 2-sides held, (c) circular clamp and (d) diamond clamp.

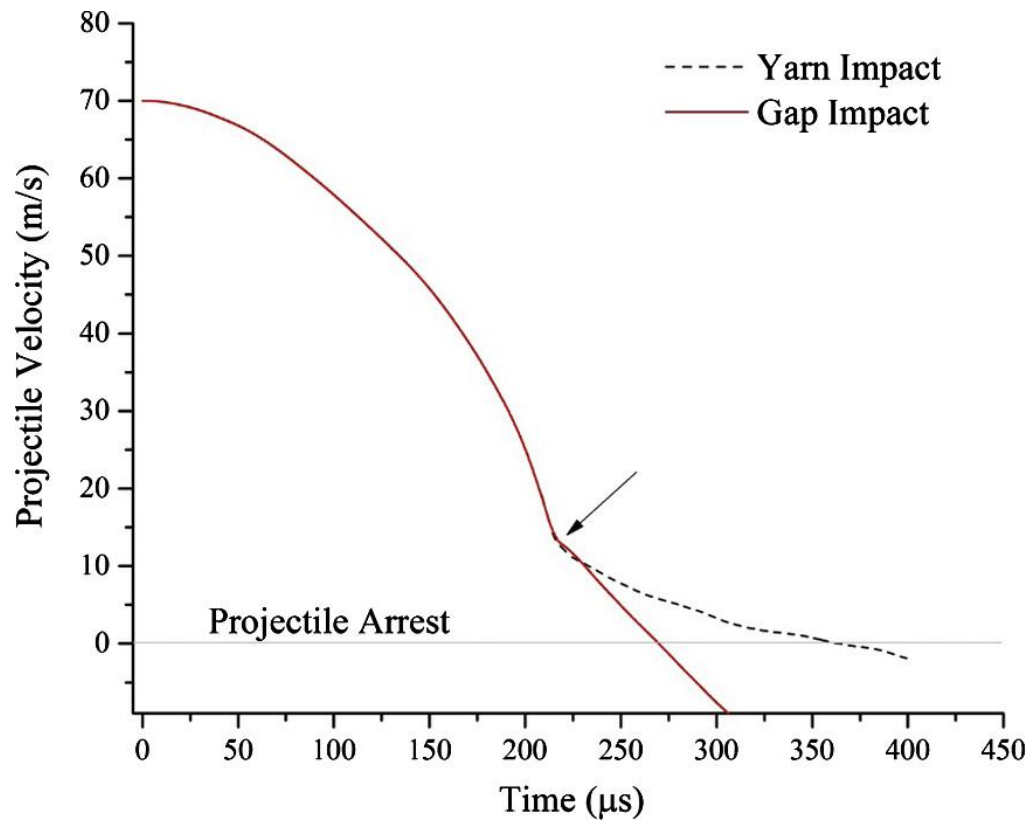


**Fig. 3.** Projectile velocity history for 2-sides held case at  $V_i$  of 70 m/s.

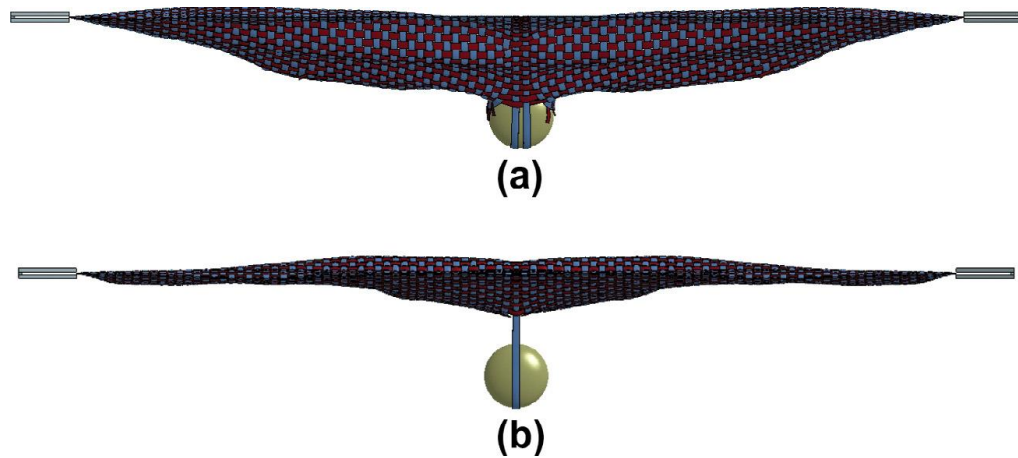


**Fig. 4.** Fabric deformation states for 2-sides held case at  $V_i$  of 70 m/s (a) gap impact at  $t = 270 \mu s$  and (b) yarn impact at  $t = 360 \mu s$ .



For the 4-sided, circular, and diamond cases, the magnitude of dissipated energy first grows to a peak value and then starts to reduce with increasing impact velocities (see Fig. 2). Because both the warp and fill yarns are constrained at both their ends, there is no yarn pullout in these impacts. The yarn impacts generally result in a greater magnitude of peak energy dissipated. Interestingly, for each of these clamping configurations, the peak dissipated energy always occurs at impact velocities greater than the  $V_{50}$  velocity.

Fig. 5 displays the 6-shot  $V_{50}$  velocities for all four clamp configurations. The circular clamp has the highest  $V_{50}$  velocity at 91.3 m/s, followed closely by the diamond clamp at 90.0 m/s. The 4-sided clamp follows at 83.8 m/s, while the 2-sided clamp has the lowest  $V_{50}$  velocity at 77.5 m/s. Fig. 6 compares the yarn impact- and gap impact-based  $V_{50}$  velocities. The circular clamp shows no sensitivity in the  $V_{50}$  velocity to precise projectile impact location, while the 4-sides clamp exhibits the greatest sensitivity.

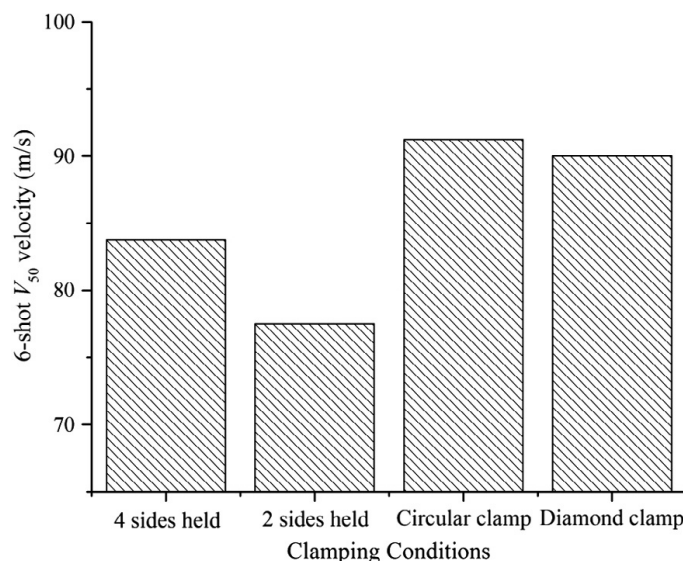


**Fig. 5.**  $V_{50}$  velocities.

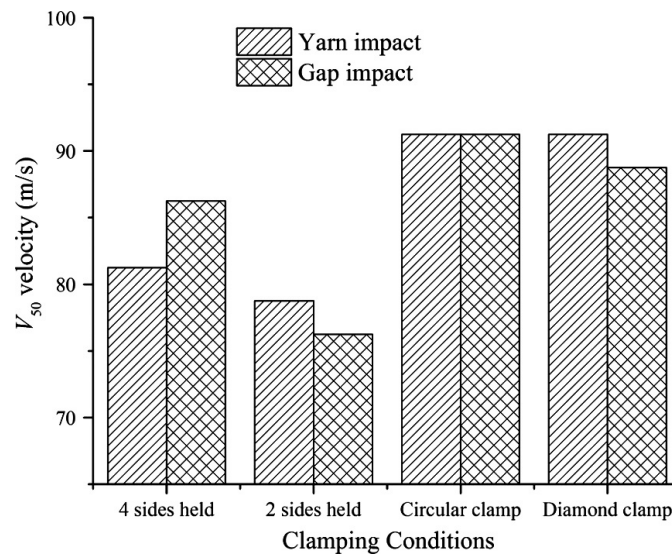


**Fig. 6.** Effect of precise impact location on V50 velocities.

Fig. 7 displays the results for a yarn impact at 80 m/s for the 4- sided, circular, and diamond clamped fabrics. The results include the time histories of projectile velocity, fabric dynamic deflection at the impact site, fabric internal energy, fabric kinetic energy, and inter-yarn frictional sliding energy. All three test shots were non-penetrating impacts. The 4-sided clamp arrests the projectile in the shortest time with the least amount of fabric deflection. The fabric internal energy primarily arises from longitudinal tensile straining of the yarns, given that the yarn tensile modulus is orders of magnitude greater than the other moduli. The principal yarns at the impact site are elongated and stressed to the highest values. They also result in the largest contributions to the fabric internal energy dissipation, which drops in the neighboring yarns with distance away from the impact site. Only the portions of the yarn behind the front of the longitudinal strain wave experience stress, while the portions ahead of the wave front have no information as yet of the oncoming strain wave. The fabric kinetic energy arises from momentum transfer between the projectile and the fabric. The fabric deforms in the shape of a pyramid, the diamond- shaped base of which represents the four



fronts of the transverse displacement wave. Only the regions of fabric behind these fronts are accelerated in the direction of the projectile resulting in the fabric kinetic energy. The kinetic energy component due to inward material flow, i.e., the inward pulling of the yarn material behind the front of the longitudinal strain wave, is negligible. The longitudinal strain wave travels much faster than the transverse displacement wave, and each interaction between the waves results in an acceleration of the transverse displacement wave front. Both waves reflect off the perfectly clamped boundaries.

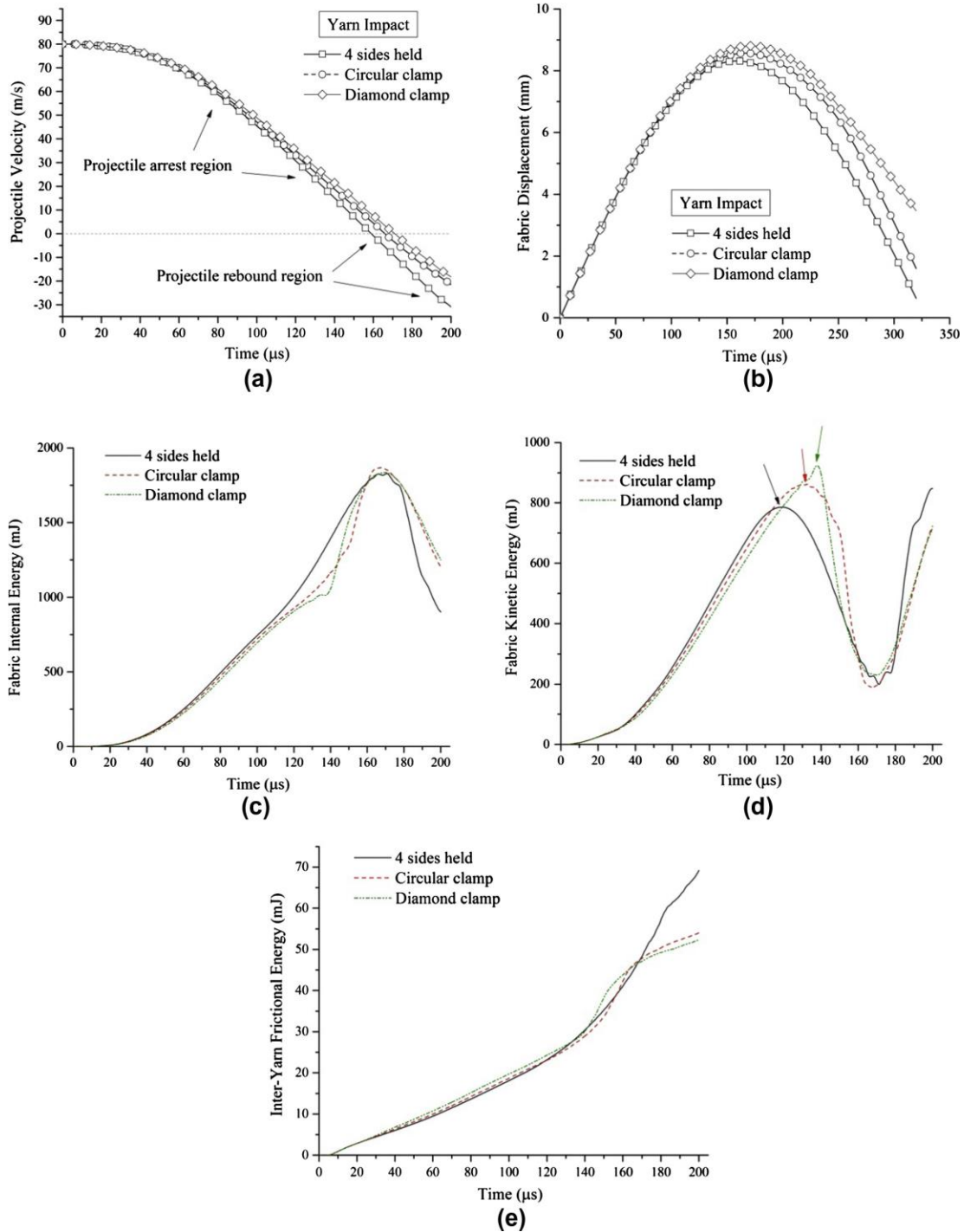


**Fig. 7.** Yarn impact at  $V_i$  of 80 m/s (a) projectile velocity, (b) fabric dynamic deflection, (c) fabric internal energy, (d) fabric kinetic energy and (e) inter-yarn frictional energy.



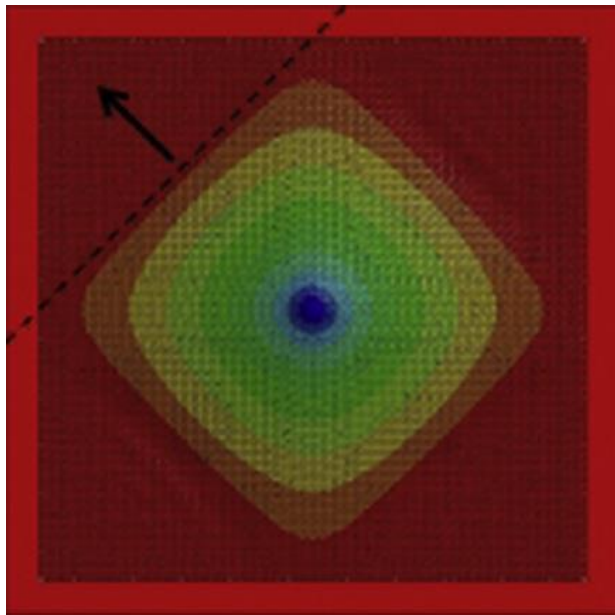


This reflection of the transverse displacement wave from the clamped boundaries is evident from Fig. 7d, and is denoted by the arrows. The fabric kinetic energy initially grows continually as the transverse wave propagates outwards and reaches a maximum value just before the wave reflects off the boundaries and starts propagating back towards the impact site. During this time, the base of the pyramidal deformation shrinks in size, and the fabric kinetic energy starts to drop in magnitude. The transverse displacement wave reflection can also be observed in Fig. 7c, where the fabric internal energy shows a sudden sharp rise in magnitude as the wave reflects off the clamped boundaries. Fig. 7e displays the inter-yarn frictional energy, which is negligible in comparison with the internal and kinetic energies for the 4-sided, circular, and diamond clamped fabrics.

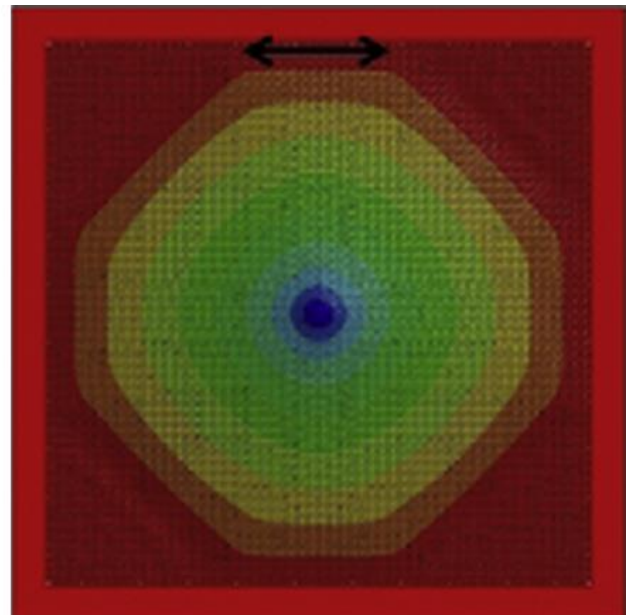
Figs. 8–10 display the contours of fabric dynamic deflection (along the direction of the projectile) at various times for a yarn impact at 80 m/s for the 4-sided, circular, and diamond clamp configurations respectively. The propagation of the transverse displacement wave is clearly observable from these contour plots, with only the fabric region behind the fronts displaced vertically. The base of the deformation pyramid remains diamond in shape for all three clamp configurations until the transverse wave interacts with a clamped boundary. For the 4-sided case, at a time instant of 130  $\mu$ s, the transverse wave has reflected from the clamped boundaries and started propagating back towards the impact site. However, as indicated by the double-headed arrow, the transverse fabric deflection has also started spreading along the clamped boundary. The projectile has been completely arrested by  $\sim 160 \mu$ s, the fabric deflection has spread over the entire exposed fabric area, and the contours of deflection have assumed its shape. Similar trends are observed for the circular clamped configuration. The contours of displacement remain diamond in shape until the transverse wave reaches the clamped boundary. After that, the contours assume a more circular configuration



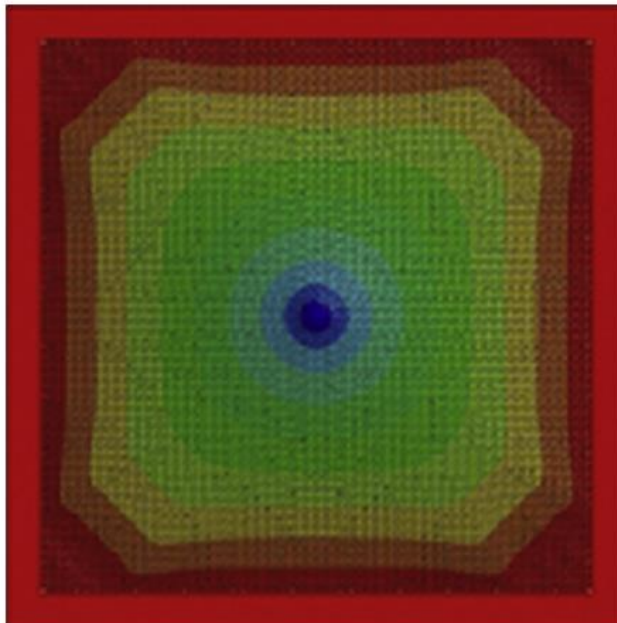
similar to the shape of the exposed fabric. By 170  $\mu$ s, the projectile has been completely arrested and starts to rebound. During the rebound, interestingly, the contours of fabric displacement once again return to being somewhat diamond in shape, as shown in Fig. 9 at 230  $\mu$ s. Similar trends are once again seen for the diamond clamped configuration in Fig. 10, where the contours of displacement are initially diamond in shape. However in this case, because the exposed fabric area is also diamond in shape, the final shape of the contours at the time of projectile arrest is also diamond-shaped and continues in that form as the projectile rebounds.



Time 110  $\mu$ s



Time 130  $\mu$ s



Time 160  $\mu$ s

**Fig. 8.** Yarn impact at  $V_i$  of 80 m/s – contours of fabric deflection for 4-sides held.

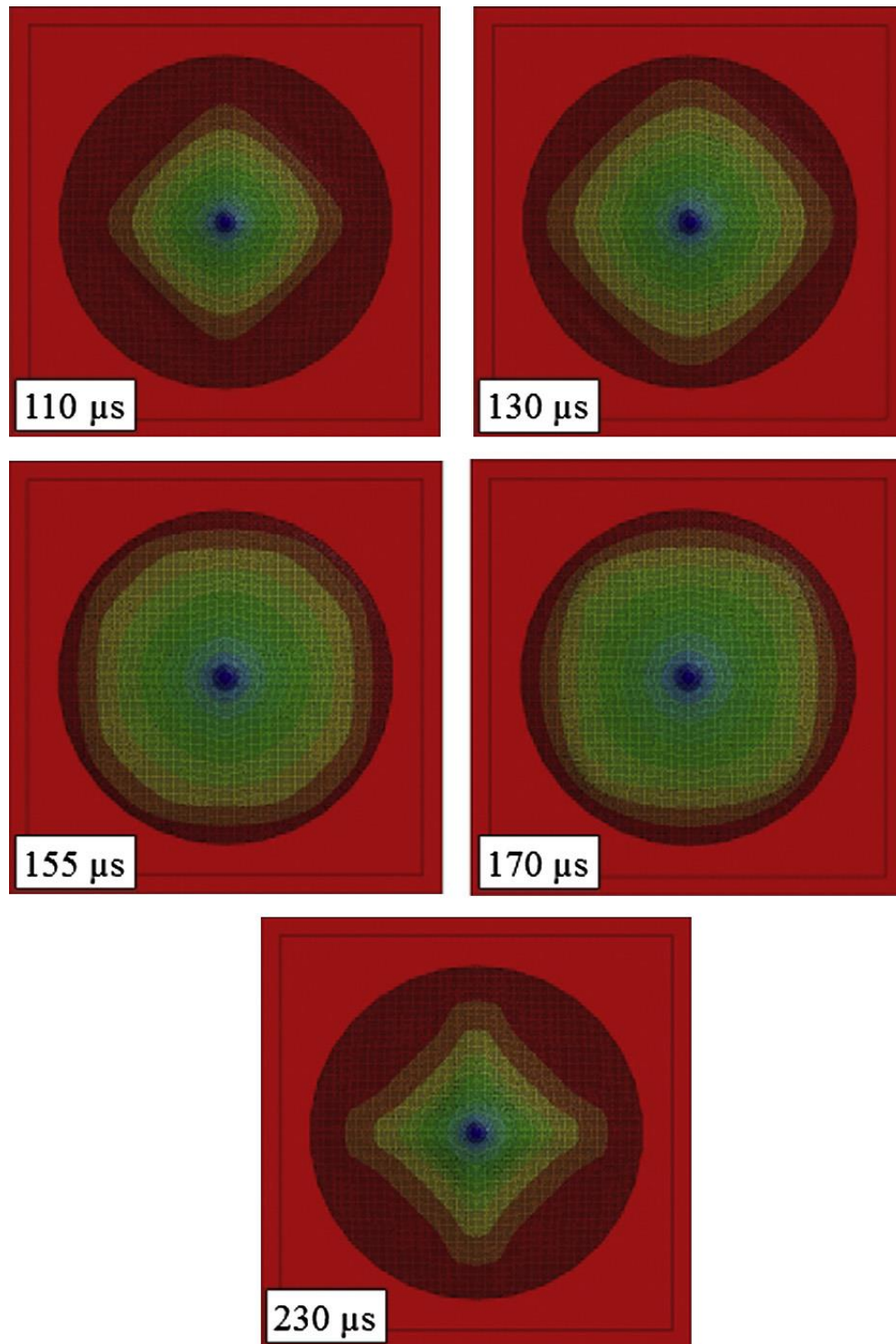


**Fig. 9.** Yarn impact at  $V_i$  of 80 m/s – contours of fabric deflection for circular clamp.

Please cite this article as: Nilakantan G, Nutt S. *Effects of clamping design on the ballistic impact response of soft body armor*. Composite Structures 108 (2014) 137–150. DOI: <http://dx.doi.org/10.1016/j.compstruct.2013.09.017>

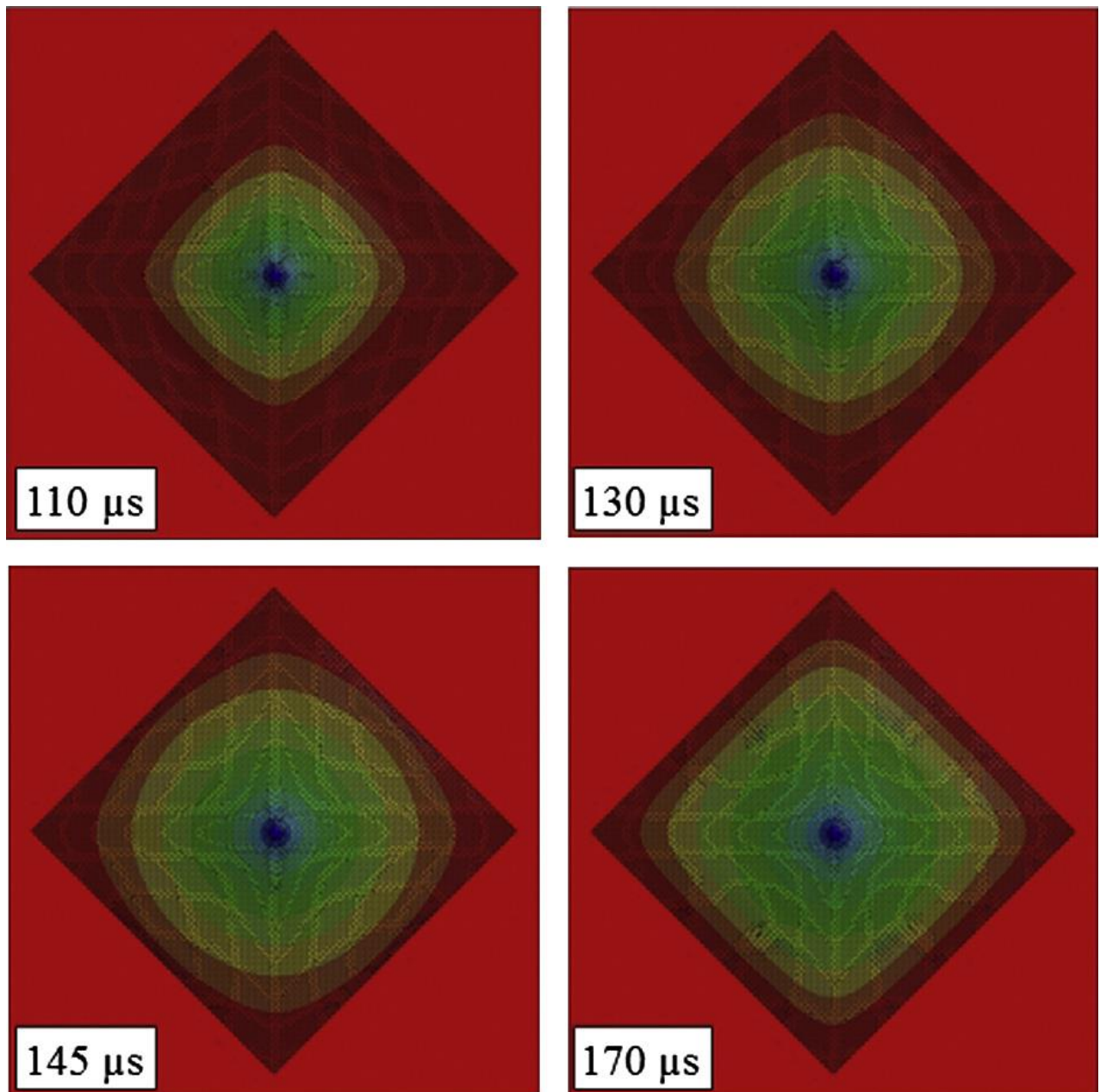


**Fig. 10.** Yarn impact at  $V_i$  of 80 m/s – contours of fabric deflection for diamond clamp.

These contour plots provide insight into the shapes and magnitudes of the fabric kinetic energy histories in Fig. 7d. Because the diamond shape of the pyramidal deformation most closely matches the exposed fabric area shape for the diamond clamped fabric, the fabric kinetic energy plot shows a sharply defined peak for the diamond clamp and only a smooth peak for the 4-sided clamp. Next

Please cite this article as: Nilakantan G, Nutt S. *Effects of clamping design on the ballistic impact response of soft body armor*. Composite Structures 108 (2014) 137–150. DOI: <http://dx.doi.org/10.1016/j.compstruct.2013.09.017>





we observe that the peak magnitudes of the fabric kinetic energy are highest for the diamond clamp. Once again, this is because of the similarity in shape between the contours of displacement and the exposed fabric area. Therefore, a larger percentage of the exposed fabric area remains behind the fronts of the transverse wave. As explained earlier, it is only the portion of the fabric behind the fronts of the wave (i.e., within the diamondshaped base of the pyramidal deformation) that are accelerated in the direction of the projectile and predominantly affect the fabric kinetic energy. However, for the 4-sided clamp, there are four triangular-shaped corner regions (i.e., far-field regions) that remain outside the fronts of the transverse wave, and therefore the percentage of exposed fabric area that predominantly contributes to the fabric kinetic energy is smaller. Although the contours of vertical displacement ultimately assume the entire shape of the exposed fabric, the contribution to the overall fabric kinetic energy is much smaller for the fabric regions outside of the diamond-shaped pyramidal deformation. Stated differently, the diamond clamp configuration allows for the largest possible size of the diamondshaped base of the pyramidal deformation before the transverse displacement wave interacts with a clamped boundary.

Fig. 11 shows contours of longitudinal yarn tensile stress for the three clamp configurations at 95 ls. All three contour plots are similar, with the maximum tensile stresses in the principal warp and fill yarns, which then rapidly drop off in magnitude with distance away from the impact site in the neighboring yarns. From these plots, the peak tensile stresses for the 4-sided clamp are the highest, followed by the circular and diamond clamps. Keep in mind that while the exposed fabric areas are the same for all cases, the longest lengths of the central-most principal yarns are different for each case as follows: 4-sided (76.2 mm), circular (85.98 mm), diamond (107.76 mm). Thus, the maximum possible yarn elongation before tensile failure is smallest for the 4-sided clamp. Moreover,

Please cite this article as: Nilakantan G, Nutt S. *Effects of clamping design on the ballistic impact response of soft body armor*. Composite Structures 108 (2014) 137–150. DOI: <http://dx.doi.org/10.1016/j.compstruct.2013.09.017>



the longitudinal strain wave reaches and reflects off the clamped boundaries most quickly for the 4-sides held clamp. Each reflection of the strain wave from the boundaries results in a spike in the yarn tensile stresses. Therefore, for the 4-sided clamp, the principal yarns reach their tensile strength more quickly than in the circular and diamond clamp configurations and consequently fail the earliest.



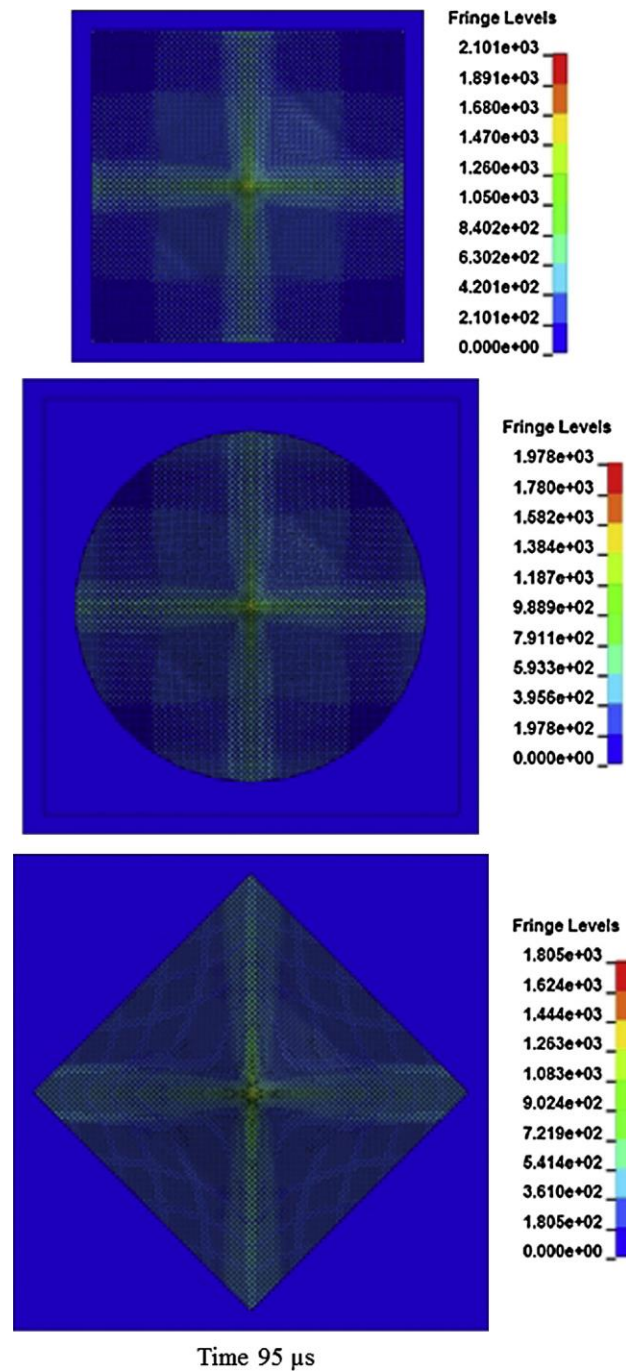


**Fig. 11.** Yarn impact at  $V_i$  of 80 m/s – yarn axial tensile stress at  $t = 95 \mu s$  for 4-sides held, circular clamp, and diamond clamp.



It is now apparent why the 4-sided clamp configuration results in the fastest projectile deceleration yet lowest fabric  $V_{50}$  velocity, while the circular and diamond clamp configurations result in the highest  $V_{50}$  velocities. The principal yarns for the 4-sided clamp fail the earliest leading to lower levels of fabric internal energy. Once these yarns fail, the structural integrity of the fabric is compromised, and the projectile can quickly penetrate through the fabric. The fabric kinetic energy is built up to larger levels for the circular and diamond clamp configurations, given that the shape of the base of the pyramidal deformation profile more closely matches the exposed fabric area. The fabric kinetic energy also rises to larger levels because the principal yarns fail later, thus maintaining fabric structural integrity longer.

Fig. 12 displays the projectile velocity and fabric energy transformation histories for a gap impact at 100 m/s for the 4-sided, circular, and diamond clamp configurations. These three test shots are all penetrating impacts. The trends follow those of the previously described non-penetrating 80 m/s yarn impact test shots. The fabric kinetic energy peak is most sharply defined for the diamond clamp and grows to the highest magnitude. The principal yarns fail earliest for the 4-sided clamp, resulting in the highest projectile residual velocity and lowest level of fabric internal energy, while the diamond clamp shows the lowest projectile residual velocity and highest level of fabric internal energy. Finally, the rate of projectile deceleration is greatest for the 4-sided clamp.

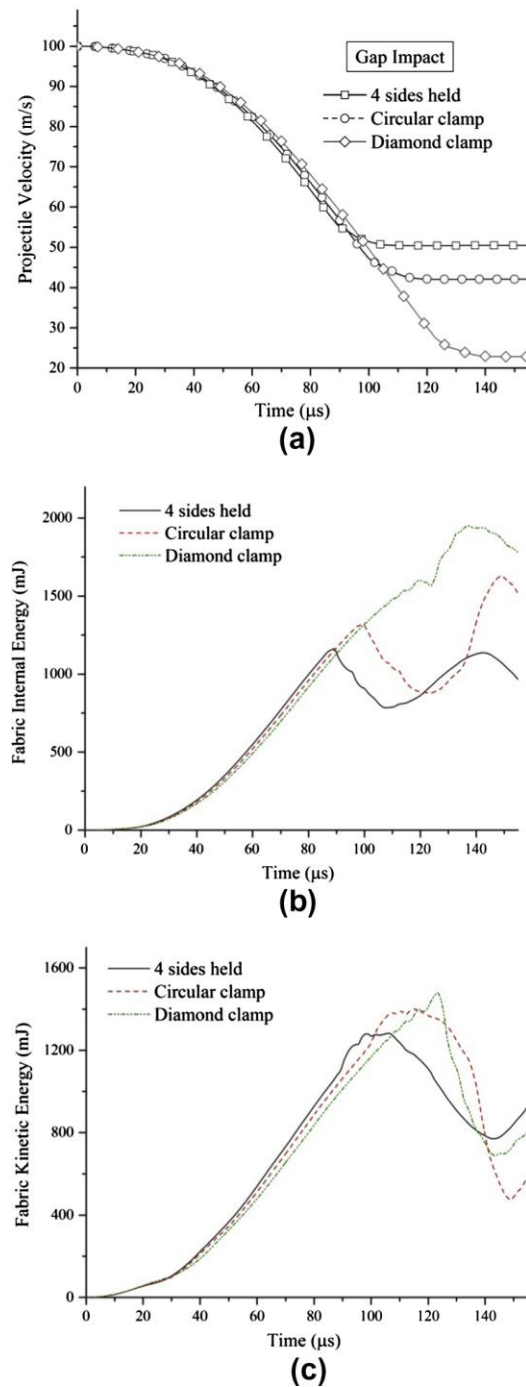
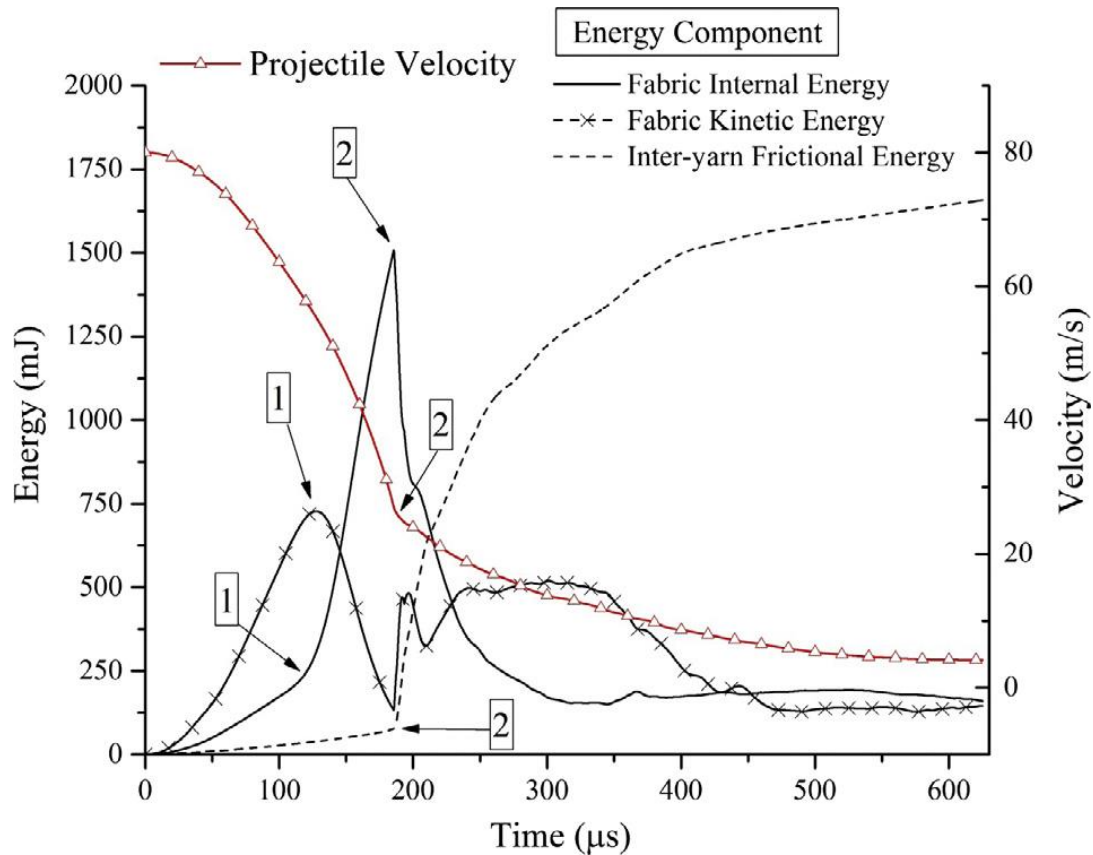


Fig. 12. Gap impact at  $V_i$  of 100 m/s (a) projectile velocity, (b) fabric internal energy and (c) fabric kinetic energy.



### 3.2 2-sided clamped fabrics

Fig. 13 displays the projectile velocity and fabric energy transformation histories for a yarn impact at 80 m/s for the 2-sided clamp configuration. There are two important time instants during this impact event, denoted by arrows '1' and '2' in Fig. 13. At  $\sim 120 \mu\text{s}$ , the transverse displacement wave reaches the clamped boundaries, causing a sharp rise in the fabric internal energy and corresponding drop in the fabric kinetic energy. At  $\sim 185 \mu\text{s}$ , the principal warp yarns fail in tension. This causes a sharp drop in the fabric internal energy, a spike in the inter-yarn frictional sliding energy, and a significant reduction in the projectile deceleration. The spike in frictional energy is caused by pulling out of the central-most fill yarn from the fabric weave. This pull-out continues until the projectile residual velocity plateaus to  $\sim 4.1 \text{ m/s}$ . Fig. 13 shows that this frictional pull-out, which is only due to a single fill yarn, results in significant energy dissipation that is roughly comparable to the fabric internal energy.



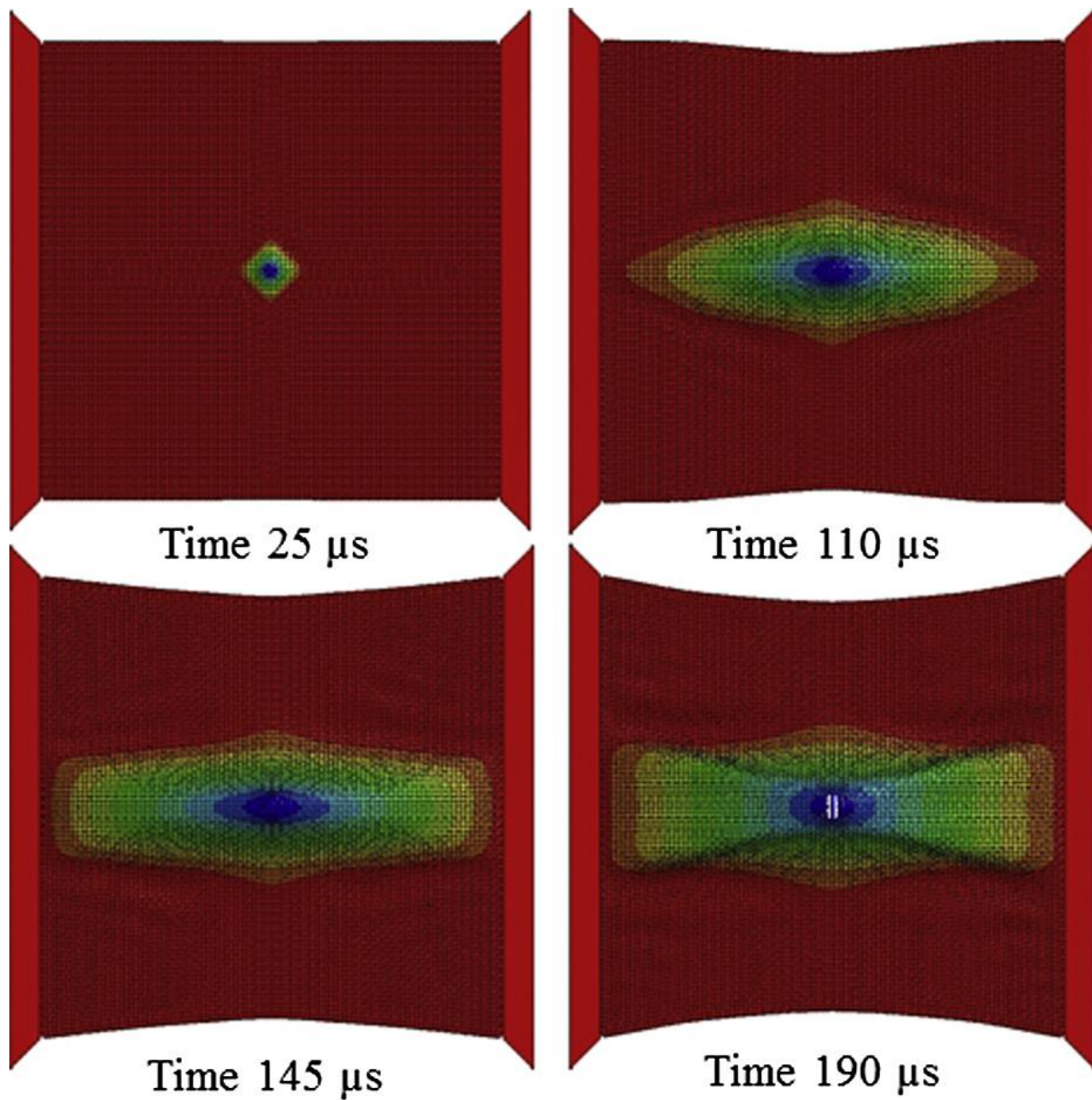
**Fig. 13.** Yarn impact at  $V_i$  of 80 m/s – projectile velocity and energy transformation histories for 2-sides held.

Fig. 14 shows contours of fabric deformation in the direction of the projectile. The deformation contour is initially diamond-shaped, as expected (see 25  $\mu$ s). However, the contour quickly elongates in the direction of the warp yarns (see 110  $\mu$ s). The fill yarns are unclamped, and the free edges of the fabric are pulled towards the impact site from the moment the longitudinal strain wave reaches the free edges. At ~145  $\mu$ s, the transverse displacement wave has started to propagate back towards the impact site, and the deformation contours also slowly spread along the clamped boundaries. These result in a somewhat rectangular displacement contour as viewed from



the top, which quickly transitions into a horizontal hourglass shape (see 190  $\mu$ s). At  $\sim 190 \mu$ s, the transverse displacement wave returns to the impact site, and a few warp yarns fail in tension. Fig. 15 shows the in-plane displacement contours of the fabric (fabric pull-in from the free edges), the yarn axial tensile stresses, and the fabric deformation state at 185  $\mu$ s. The fabric deformation and loading appear to be confined within a rectangular patch that runs all the way from the left clamp to the right clamp. Outside this patch, the warp and fill yarns do not develop significant stress levels. Thus for the 2-sided clamp configuration, the degree of deformation and loading is spatially non-uniform over the entire exposed fabric area. Only a small rectangular-shaped patch of fabric at the center significantly contributes to the initial larger overall energy dissipation (from  $V_i = 80$  m/s to  $V_{inst} = 26$  m/s). This is followed by the fill yarn frictional pullout from the weave that dominates the subsequent smaller overall energy dissipation (from  $V_{inst} = 26$  m/s to  $V_r = 4.1$  m/s).





**Fig. 14.** Yarn impact at  $V_i$  of 80 m/s – contours of fabric deflection for 2-sides held.



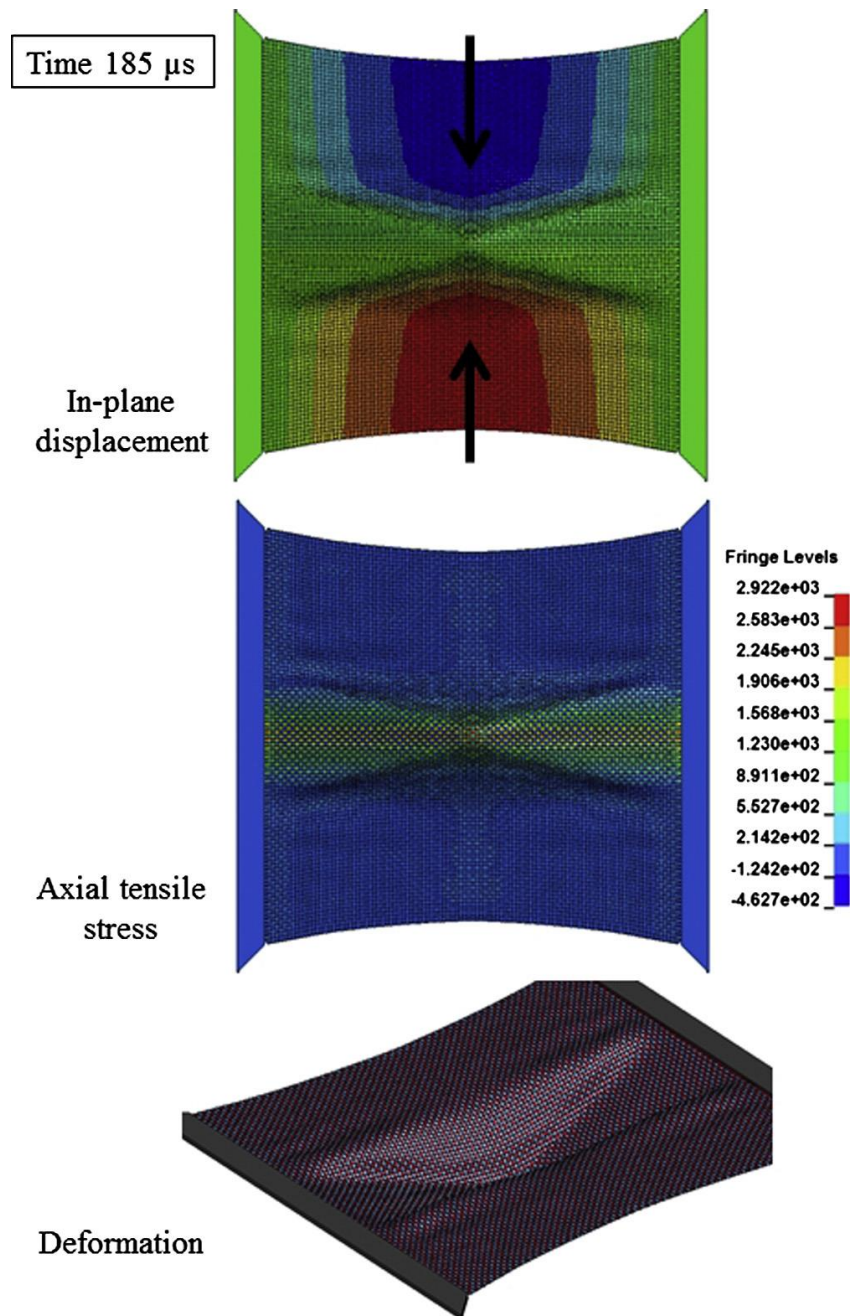


**Fig. 15.** Yarn impact at  $V_i$  of 80 m/s – contours of in-plane displacement and axial tensile stress, and deformation state for 2-sides held at  $t = 185 \mu$ s.



Fig. 16 shows two more deformation states for the 2-sided clamp configuration at 285  $\mu\text{s}$  and 625  $\mu\text{s}$ , both of which are within the regime of fill yarn pullout. A large extent of fabric creasing is apparent in Fig. 16a. During the frictional fill yarn pullout, the fabric region which had initially been vertically displaced along the direction of the projectile (i.e. pyramidal deformation) begins to rebound to its original position. By 625  $\mu\text{s}$ , the projectile has reached a steady residual velocity. The fabric has returned to its original position, and the creasing has extended to the entire exposed area of the fabric.

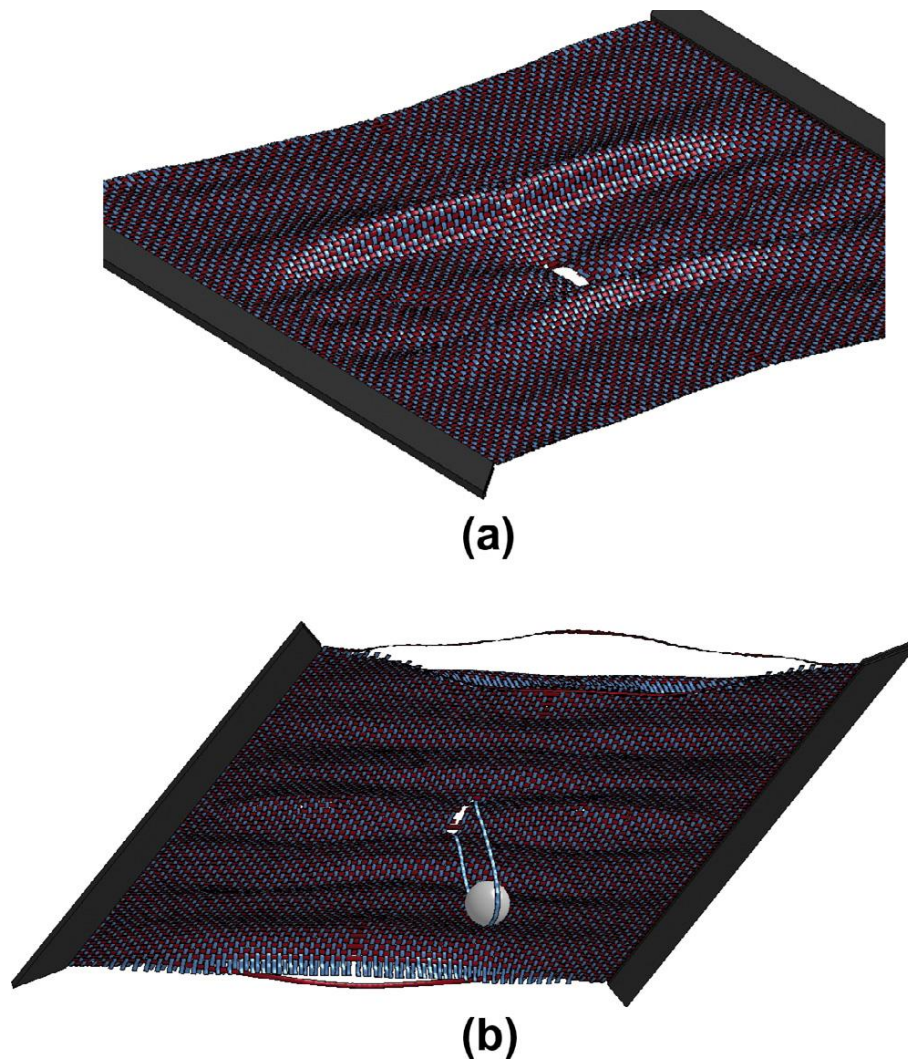




**Fig. 16.** Yarn impact at  $V_i$  of 80 m/s – fabric deformation states for 2-sides held at (a)  $t = 285 \mu\text{s}$  and (b)  $t = 625 \mu\text{s}$ .

### 3.3 Corner plate clamped fabrics

The various regions of interest for the corner plate clamped fabric are shown in Fig. 17, all of which have the same exposed fabric area. The projectile velocity history is shown in Fig. 18, as well as the internal energy histories for each of the five fabric regions of interest. The center region develops internal energy more quickly than the other four regions at the top, bottom, left, and right. Clearly, such a clamp design is not desirable, since the area of the center region can be made larger while reducing the areas of the other four regions such that the total exposed fabric area remains the same. However, in such a case, the fabric would have a completely different impact response. The corner plate clamped fabric appears to be a combination of two other clamp configurations, although in reality it is much more complex than that. The central region appears to be in an approximately corner point clamp configuration, while the other four regions appear to be in 2-sided clamp configurations. The shared edges between the center region and the four surrounding regions act as partially constrained boundaries, whose compliance is partially governed by the dimensions of the four surrounding regions.



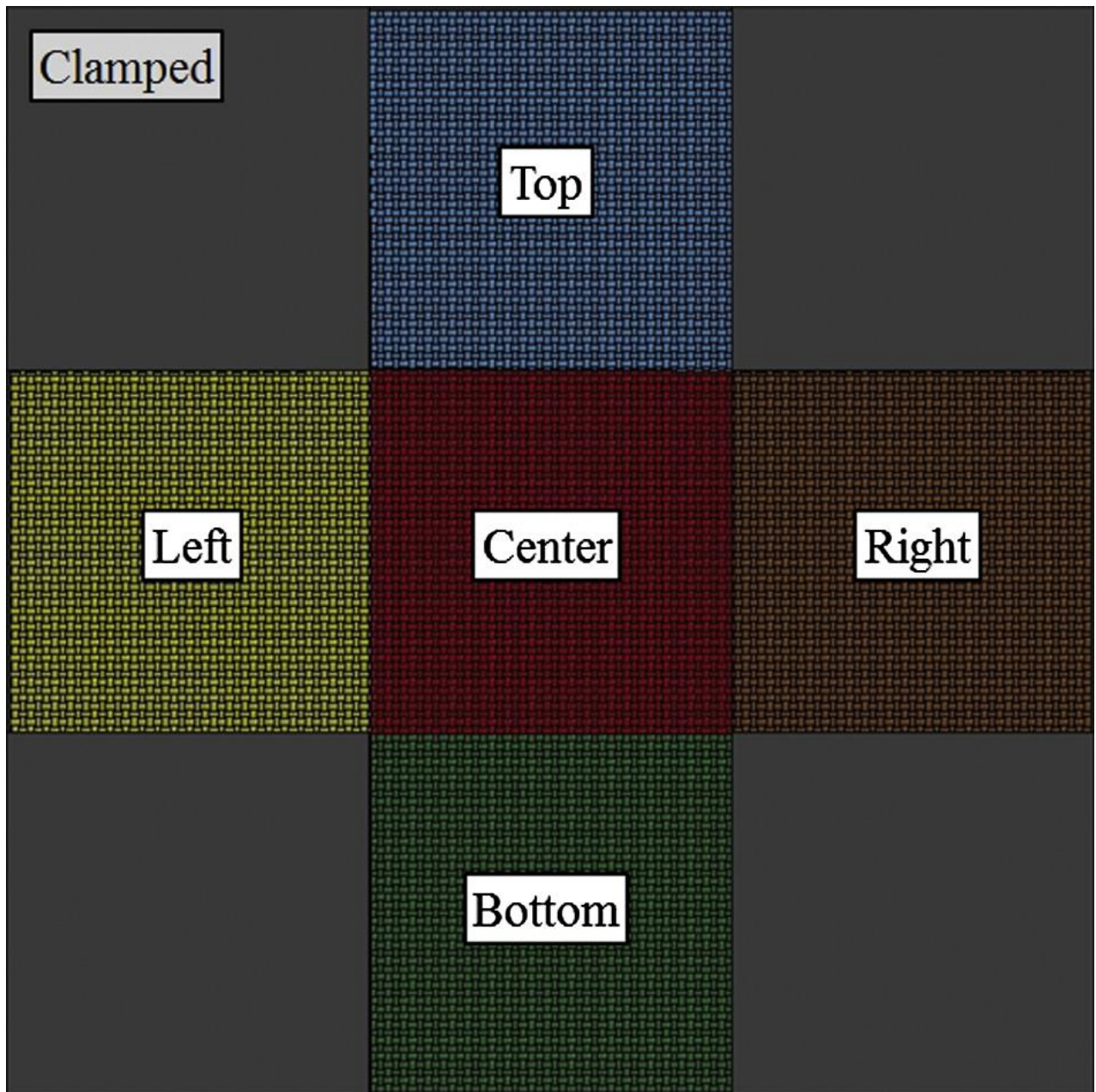


*Fig. 17. Regions of interest for the corner plate clamp.*

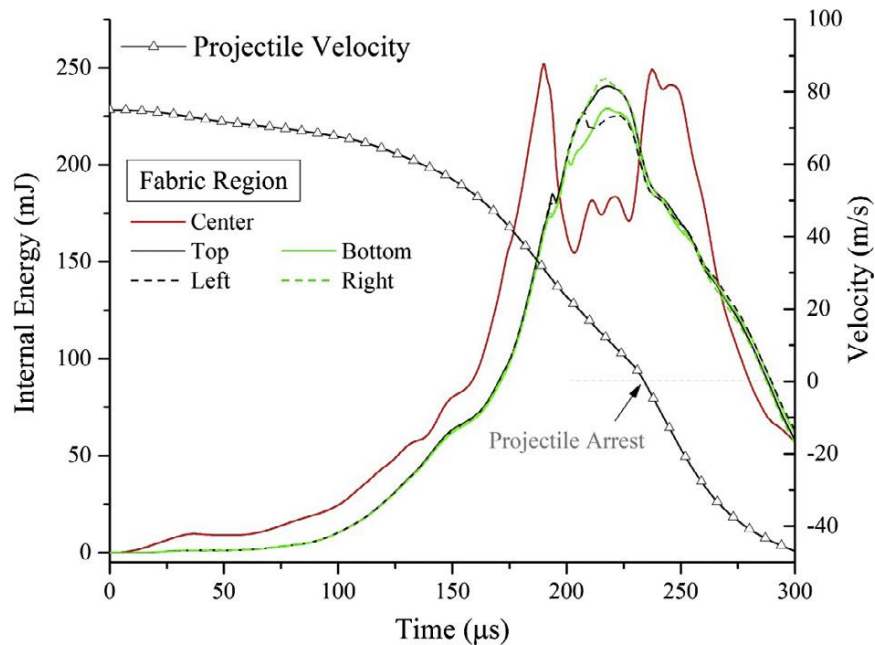


**Fig. 18.** Yarn impact at  $V_i$  of 75 m/s – projectile velocity and energy transformation histories for corner plate clamp.

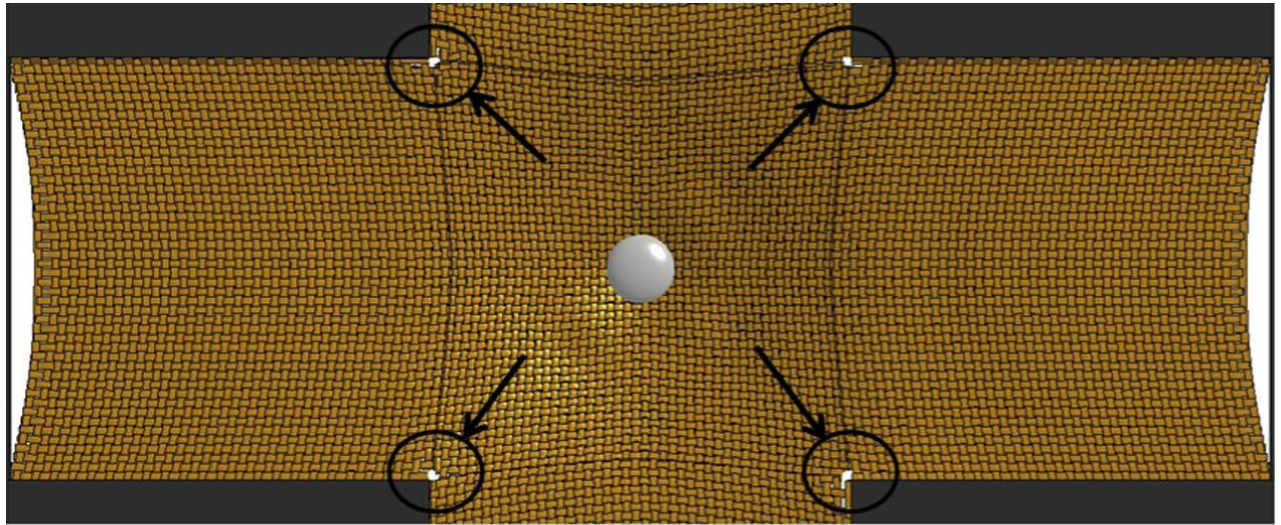
The fabric deformation state at 209  $\mu$ s is shown in Fig. 19a. Tearing occurs at the four corners of the center region of fabric. These locations are under high stress concentrations. In a corner plate clamping configuration, once the diamond-shaped base of the transverse deformation pyramid reaches a clamped boundary, fabric creasing develops because of the interactions of the wave fronts with the sharp 90° corners. Moreover, the pull-in forces exerted by the fabric on the clamped boundaries are not uniform over their length. This is another undesirable effect. In contrast, for the diamond clamp configuration, because the clamped edges are parallel to the fronts of the transverse displacement wave, the forces exerted on the clamped edges are more uniform along the length of the clamps. From Fig. 19a, inward pulling of the fabric towards the impact site is evident at the left and right edges of the fabric, while the outer-most fill yarns have separated from the weave. The



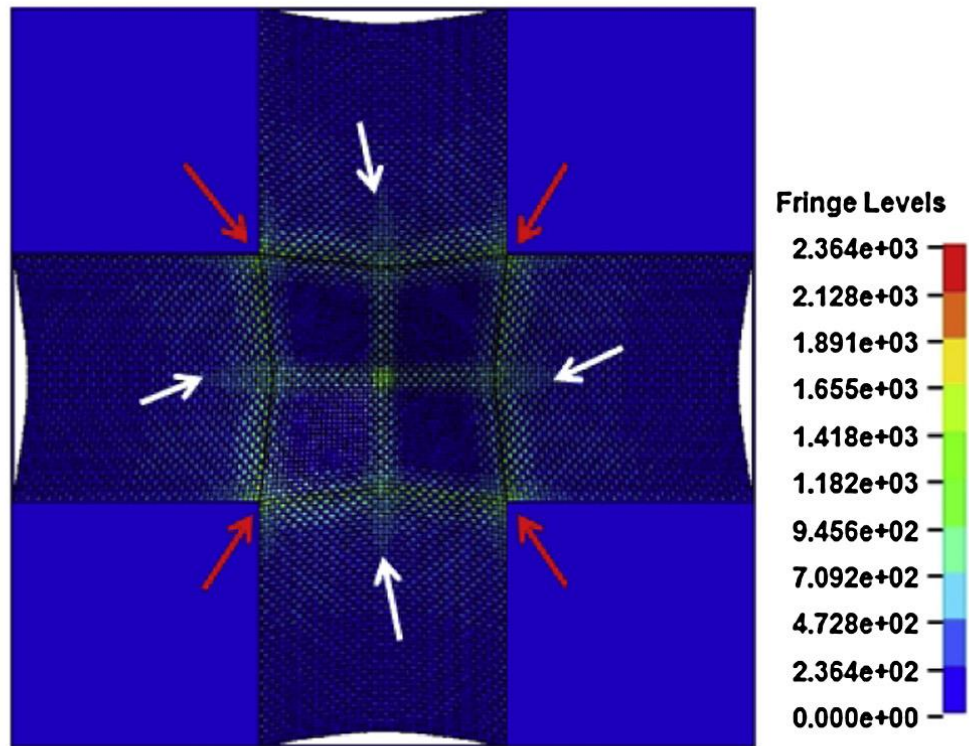
same phenomenon is observed for the top and bottom edges of the fabric where the outer-most warp yarns have separated from the weave (not shown).

Fig. 19b shows contours of the longitudinal yarn tensile stress at 190  $\mu$ s, which is just before corner tearing occurs. The fabric stress state illustrates why this clamping design is undesirable. The central principal warp and fill yarns experience extreme yarn stresses. However, as indicated by the white arrows, the entire length of the principal yarn (i.e., extending to the free edges) is not stressed, and the tensile stresses are predominantly confined to the yarn length that lies within the central region. Furthermore, narrow bands of warp and fill yarns that lie between the four red arrows are also stressed to high values comparable to the principal warp and fill yarns, while the yarns in-between experience low stress levels. This behavior is quite different from the other clamp configurations, wherein the yarn tensile stresses are highest in the centralmost principal yarns, and decline with distance from the impact site. The stress levels at the four corners of the central region (red arrows) are regions of stress concentration and experience high stress levels, resulting in fabric tearing at these corners. As shown in the figure, the far-field regions of the fabric near the free edges experience low stress levels, resulting in low-to-negligible contributions to the fabric internal energy. Because the transverse displacement wave also cannot easily reach these far field regions (without the fabric first experiencing yarn failure at the impact site or fabric tearing at the corners), the contribution of these far-field regions to the fabric kinetic energy is also low to negligible.





(a)



(b)

**Fig. 19.** Yarn impact at  $V_i$  of 75 m/s: (a) Tearing at fabric corners for corner plate clamp at  $t = 209$   $\mu$ s and (b) yarn axial tensile stress at  $t = 190$   $\mu$ s.

Please cite this article as: Nilakantan G, Nutt S. *Effects of clamping design on the ballistic impact response of soft body armor*. Composite Structures 108 (2014) 137–150. DOI:

<http://dx.doi.org/10.1016/j.compstruct.2013.09.017>





### 3.4 Corner point clamped fabrics

Plots of  $V_i-V_r$  and  $V_i-E_d$  for the corner point clamped fabric are shown in Fig. 20. The plots indicate there is no sensitivity in the impact performance to the precise projectile impact location except near one of the chosen impact velocities (i.e. 300 m/s), discussed later. The  $V_i-V_r$  plot shows a sharp increase in slope beyond an impact velocity of 200 m/s. As seen from Fig. 20a, an impact velocity of 20 m/s results in non-penetration, while 30 m/s results in penetration. Therefore, a crude estimate of the fabric  $V_{50}$  velocity for the corner point clamp configuration is 25 m/s. This is approximately the projectile impact velocity required to completely eject the bulk fabric from the two peripheral yarns at each of the four edges that are clamped at their two ends, which comprise the four corner point clamping configuration. This indicates that if the corner point clamping configuration were instead comprised of clamping three or more yarn widths at each of the four corners, then the  $V_{50}$  velocity will change accordingly. Practically, techniques such as the use of Velcro straps are used to freely suspend a fabric target to simulate a fully unclamped boundary condition. However, the  $V_{50}$  velocity is sensitive to the precise corner point clamping methodology, an issue left to future studies.

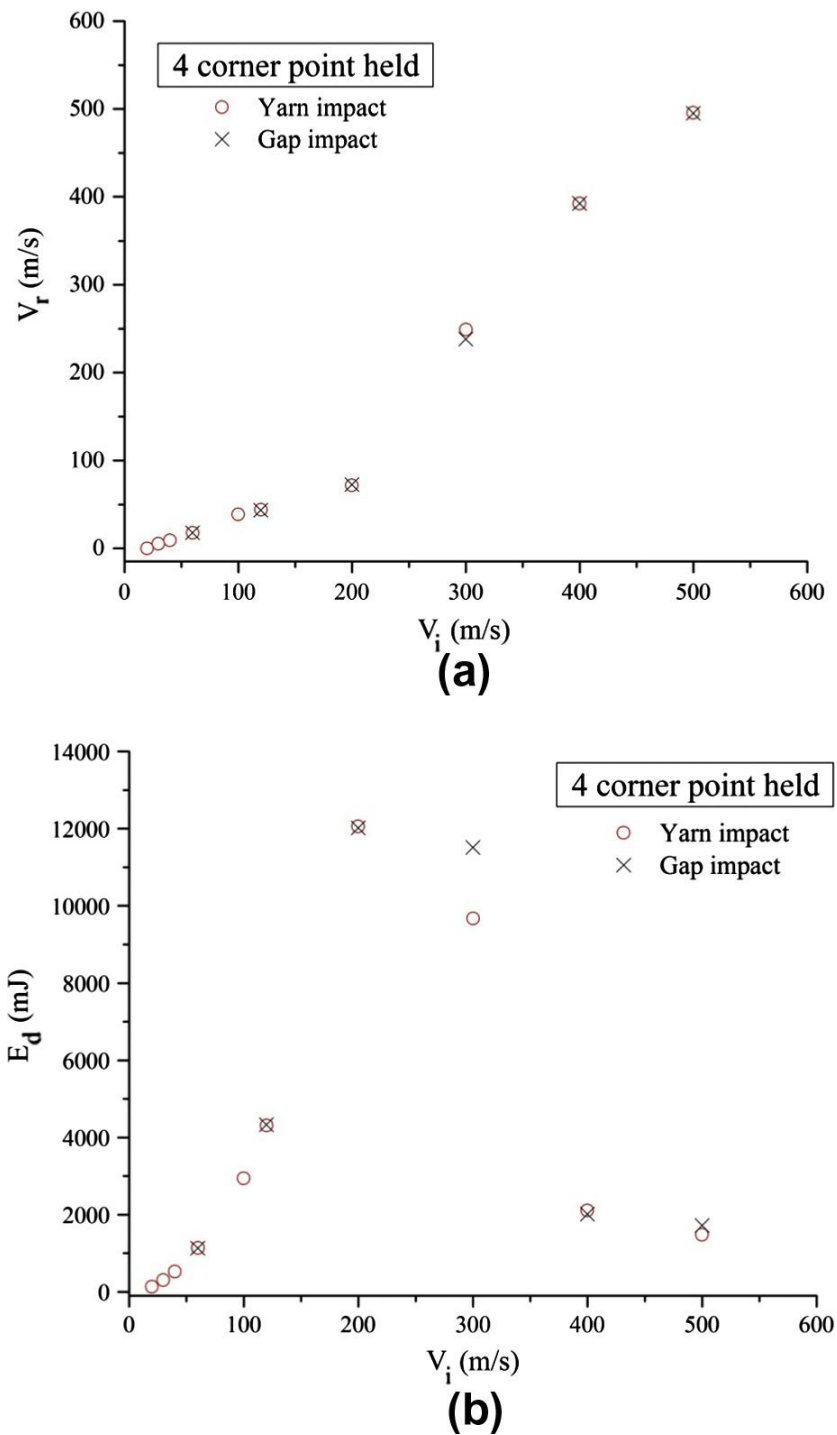


**Fig. 20.** (a) Impact vs residual velocity plot and (b) impact velocity vs energy dissipated plot for corner point clamp.

The magnitudes of dissipated energy grow rapidly with increasing projectile impact velocities up to  $\sim 200$  m/s, after which the magnitudes show a gradual but noticeable drop. However, further increases in impact velocities result in sharp drops in the magnitudes of the dissipated energies. To better understand these trends, fabric deformation states for the corner point clamp configuration at various time instants are plotted for (a) 200 m/s gap impact, (b) 300 m/s gap impact, (c) 300 m/s yarn impact, and (d) 400 m/s gap impact (Fig. 21). Furthermore, Fig. 22 shows the projectile velocity and energy transformation histories for a 200 m/s gap impact test shot, while Fig. 23 compares similar data between a yarn-based and gap-based impact for a 300 m/s test shot.

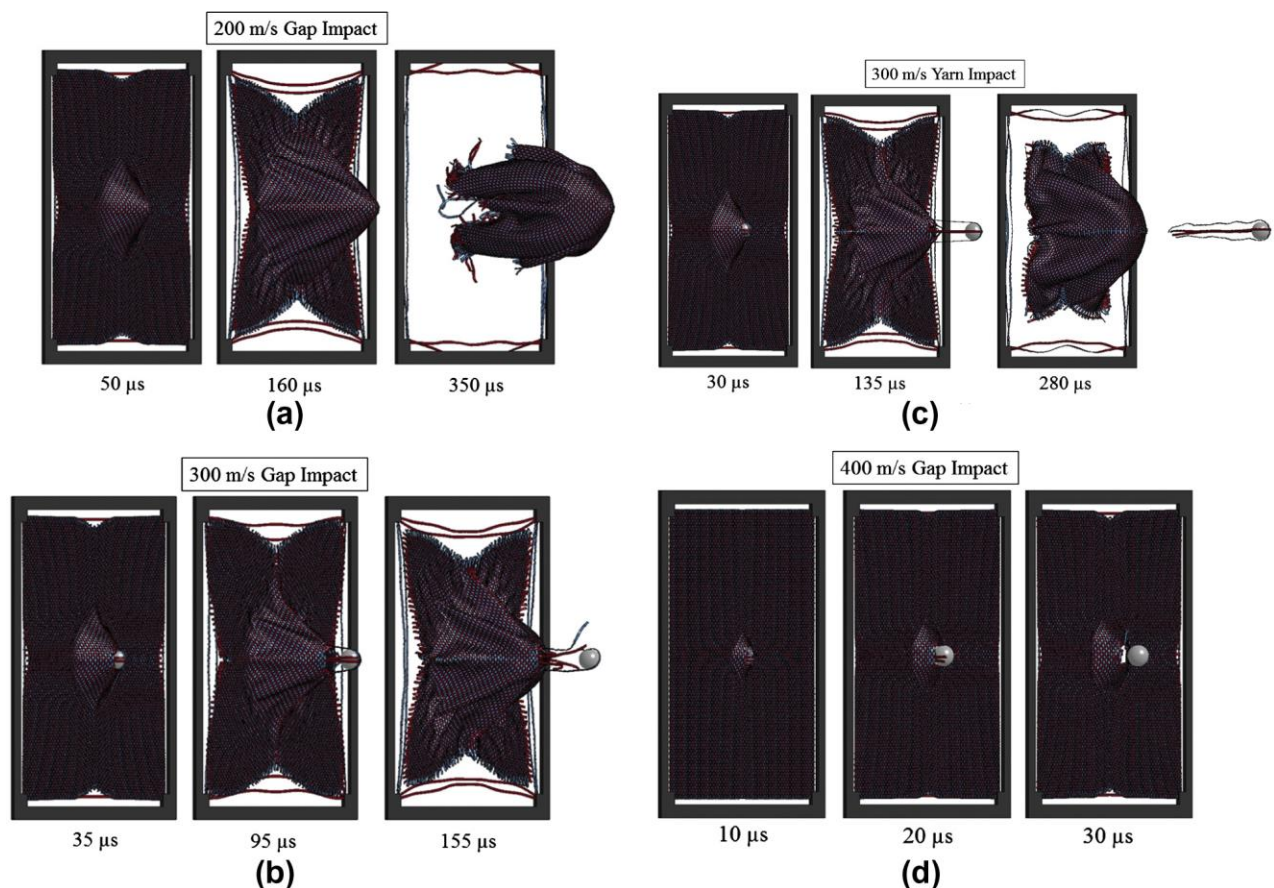


**Fig. 21.** Fabric deformation states for corner point clamp (a) gap impact at  $V_i$  of 200 m/s, (b) gap impact at  $V_i$  of 300 m/s, (c) yarn impact at  $V_i$  of 300 m/s and (d) gap impact at  $V_i$  of 400 m/s.

Please cite this article as: Nilakantan G, Nutt S. *Effects of clamping design on the ballistic impact response of soft body armor*. Composite Structures 108 (2014) 137–150. DOI: <http://dx.doi.org/10.1016/j.compstruct.2013.09.017>

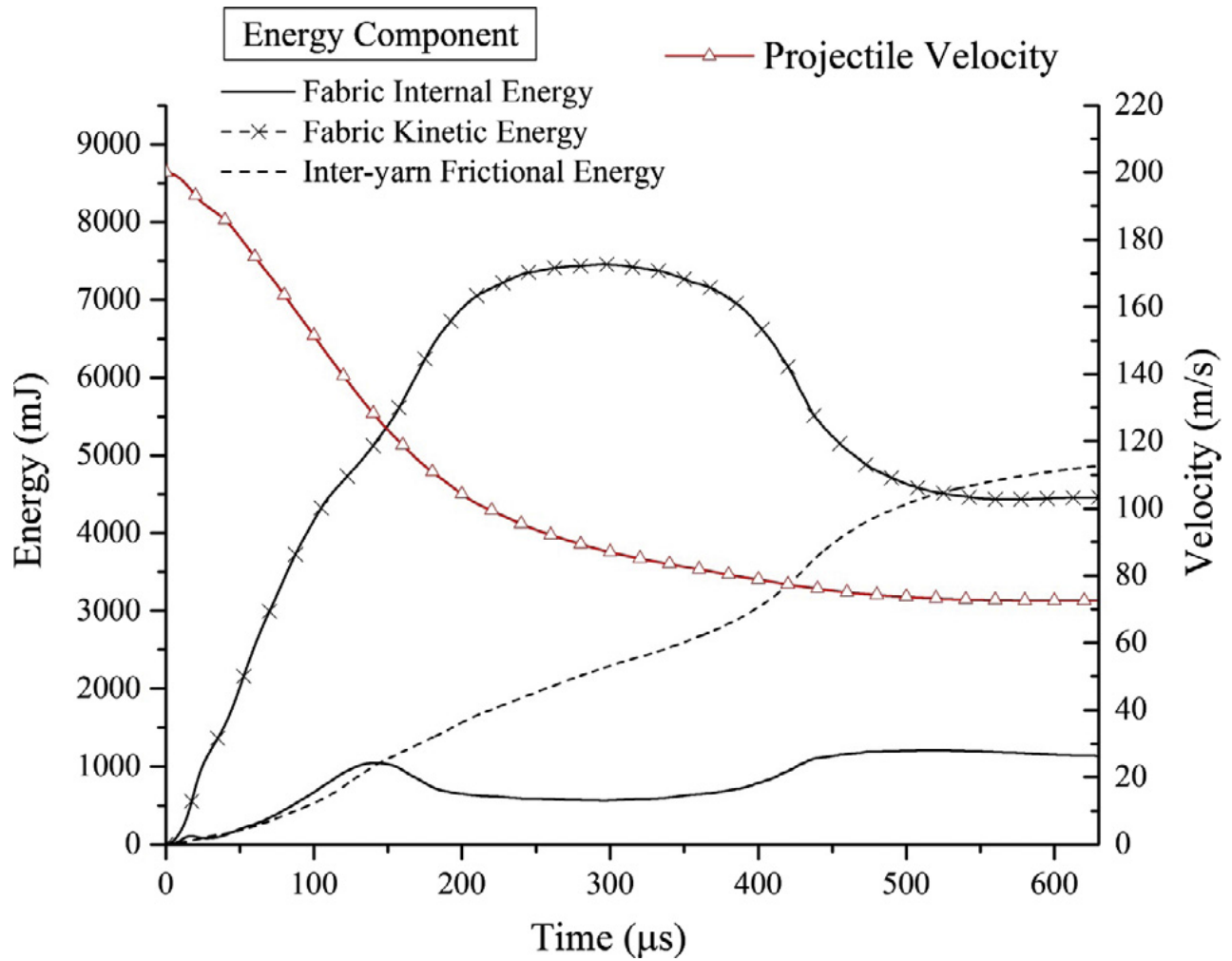
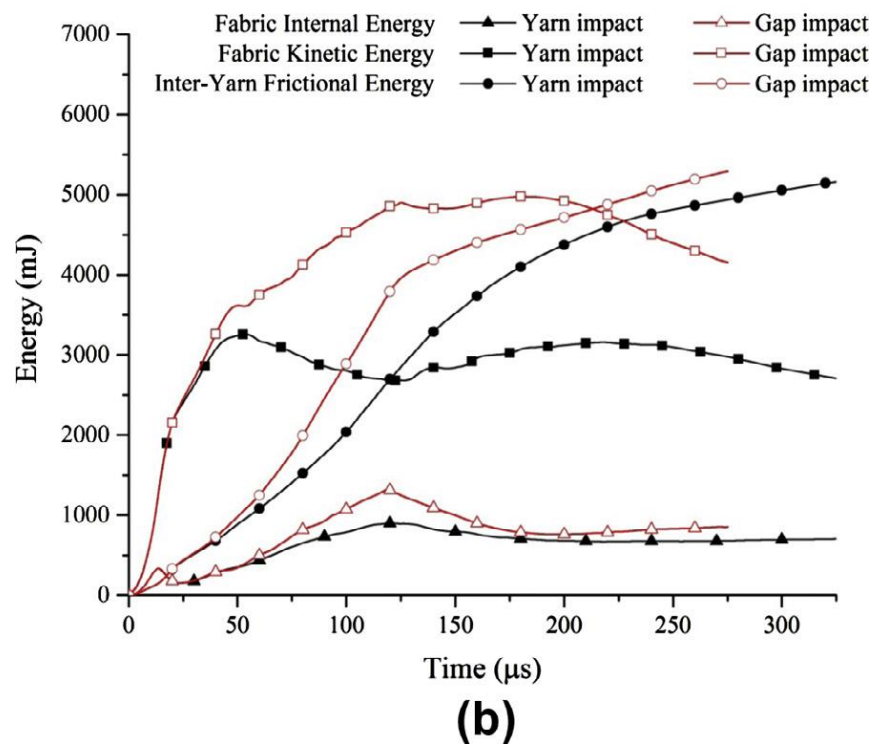
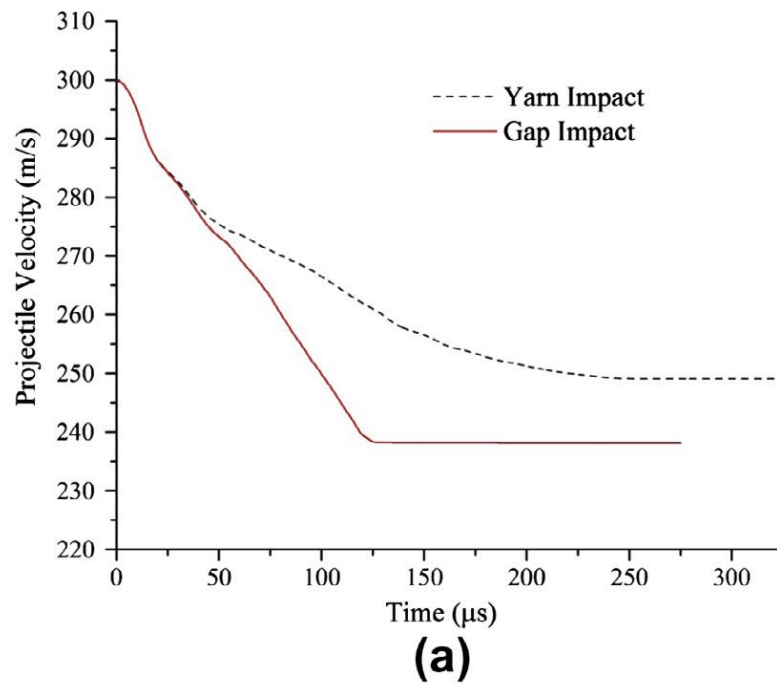


Fig. 22. Gap impact at  $V_i$  of 200 m/s – projectile velocity and energy transformation histories for corner point clamp.



**Fig. 23.** Yarn vs gap impact at  $V_i$  of 300 m/s for corner point clamp (a) projectile velocity history and (b) energy transformation history.



From Fig. 21a, up to  $\sim 200$  m/s, the entire fabric is ejected from the fixture except for two yarns at each of the four edges, which run between the clamped corner points. Initially, the base of the pyramidal deformation follows the usual diamond shape; however, creases begin to appear in the deformation pyramid because of the large extent of pull-in from the free fabric edges. Once the fabric is ejected from the fixture, it begins to wrap around the projectile and is pulled along with it. During this time, as shown in Fig. 22, the predominant source of energy dissipation that results in projectile deceleration is the momentum transfer between the projectile and bulk fabric, i.e. kinetic energy required to drag the bulk fabric along with the decelerating projectile. The magnitude of the fabric internal energy remains low in comparison, while the inter-yarn frictional energy steadily increases over time to magnitudes nearly comparable to the fabric kinetic energy. Note that this frictional energy is not due to yarn pullout, but rather due to yarn reorientation and small extents of inter-yarn sliding at the cross-over regions due to excessive fabric bending and creasing. However, at 300 m/s, we also observe yarn pullout of the principal warp and fill yarns, in addition to the entire bulk fabric once again getting ejected from the fixture. For the gap impact at 300 m/s (Fig. 21b), the two central warp and two central fill yarns start to pull out of the fabric weave (see 95  $\mu$ s). By 155  $\mu$ s, three of these yarns have failed, and only one of the principal warp yarns remains intact and continues to pull out of the weave. For the yarn impact at 300 m/s (Fig. 21c), the central-most warp and fill yarn start pulling out of the fabric weave (see 135  $\mu$ s), and this pullout of both yarns continues until they have been completely ejected from the fabric weave, as shown at 280  $\mu$ s. Fig. 23a shows the strong sensitivity of the fabric impact response to the precise projectile impact location for the 300 m/s impact test shots. Like the 2-sided clamped test shot from Fig. 3, a gap impact leads to a faster deceleration of the projectile, because a greater number of yarns are being simultaneously pulled out.

However, unlike the 2-sided case, for the corner point clamped fabric, yarn pullout is not a major

Please cite this article as: Nilakantan G, Nutt S. *Effects of clamping design on the ballistic impact response of soft body armor*. Composite Structures 108 (2014) 137–150. DOI:

<http://dx.doi.org/10.1016/j.compstruct.2013.09.017>



source of energy dissipation. The frictional energy dissipated depends on the frictional pullout force and the distance over which the yarn is pulled out. The former depends on the inter-yarn normal contact force at the yarn crossover. Typically, for large contact forces to develop, at least two sides of the fabric or sufficient areas at the four corners of the fabric must be clamped. That is not the case for the corner point clamped fabric.

The point of deviation in the projectile velocity histories for the yarn and gap impact test shots in Fig. 23a occurs at  $\sim 30 \mu\text{s}$ , which corresponds to the initiation of yarn pullout after the failure of some warp and fill yarns at the impact site. Fig. 23b shows that at about this time, the fabric kinetic energy histories also deviate from one another. The fabric kinetic energy of the gap impact continues to grow, while that of the yarn impact plateaus out. This shows that the yarn pullout for the gap impact is able to pull the bulk fabric along with it to a greater extent than the yarn impact, leading to a larger pyramidal deformation, which in turn indicates greater momentum transfer between the projectile and fabric. For the yarn impact however, the central-most warp and fill yarns are more easily pulled out of the fabric weave with less resistance, leading to little further increase in the size of the fabric pyramidal deformation or fabric kinetic energy. The fabric internal energies for both yarn and gap impacts are similar in magnitude and much smaller in comparison with the fabric kinetic energies.

For the 400 m/s gap impact test shot, the yarns fail in tension almost immediately after impact, as shown in Fig. 21d. The deformation pyramid has barely formed before yarn failure at the impact site and fabric penetration by the projectile. This leads to low energy dissipation levels, as shown in Fig. 20a. The impact response is not sensitive to the precise projectile impact location, and the bulk fabric is not ejected from the fixtures.

Please cite this article as: Nilakantan G, Nutt S. *Effects of clamping design on the ballistic impact response of soft body armor*. Composite Structures 108 (2014) 137–150. DOI: <http://dx.doi.org/10.1016/j.compstruct.2013.09.017>





To summarize, three distinct velocity regimes can be observed for the corner point clamped configuration that lead to residual projectile velocities. In the ‘low velocity’ regime, the bulk fabric is ejected from the fixture and dragged along with the projectile, although there is no yarn failure or fabric penetration. This is still considered a ‘penetration’ in the conventional sense, since the projectile retains residual velocity at the end of the impact event. In the ‘mid velocity’ regime, principal yarn pullout occurs in conjunction with the bulk fabric being ejected from the fixture. This regime is highly sensitive to the precise projectile impact location (yarn or gap). In the ‘high velocity’ regime, the yarns fail in tension soon after impact, and the bulk fabric remains in the fixture. The transverse deformation pyramid does not have sufficient time to form, and there is little fabric pull-in from the four free edges. There is also little energy dissipation in this regime. For both the low-velocity and high-velocity regimes, the impact response is not sensitive to the precise projectile impact location.

## 4. Conclusions

We have demonstrated that clamp design has a significant effect on the interactions and mechanisms of fabric deformation, failure, and energy dissipation, and importantly, the V50 velocity, which is used as a predictor of ballistic impact performance. This has two important consequences:

(1) When comparing the ballistic impact performance of nonbacked soft body armor between different laboratories and/or between different target configurations, the clamping specifications are just as important as the material and threat specifications.



(2) By using different clamping designs, the various mechanisms of fabric deformation and energy dissipation can be promoted or suppressed, which allows for a systematic tailoring of the target's geometry, material, and interfaces, in turn leading to new innovations.

For example, when developing new interfaces and yarn sizing that affect the inter-yarn frictional interactions, a grip design that promotes mechanisms such as frictional yarn re-orientation and frictional yarn sliding/pullout can be used instead of the conventional 4-sided or even circular/diamond clamp configurations. While not included within the scope of this study, frictional yarn re-orientation can also be promoted by shooting bias-oriented fabrics ( $\pm 45^\circ$ ) held in a 2-sided clamp.

We have also shown that the circular clamped fabric results in the highest predicted  $V_{50}$  velocity and shows no sensitivity to precise projectile impact location, closely followed by the diamond clamped fabric. A practical consideration during experimental impact testing is the misalignment of the fabric within the grips, which could affect the impact performance, i.e., the fabric may be slightly rotated within the grips, and the yarns are not oriented precisely at 90 to the edges of the frame. This is usually a consequence of operator error. However, because of symmetry about the vertical (out-of-plane) axis, the circular clamp is not sensitive to inplane fabric rotations, giving it a slight advantage over the other clamping configurations.

Clamp designs wherein the clamped edges are oriented either nearly or exactly parallel to the fronts of the transverse displacement wave are preferable. Thus, circular or diamond clamp configurations are preferable over 4-sided, 2-sided, and corner clamp configurations. These two configurations also result in a more uniform and gradually-varying spatial distribution of fabric

Please cite this article as: Nilakantan G, Nutt S. *Effects of clamping design on the ballistic impact response of soft body armor*. Composite Structures 108 (2014) 137–150. DOI: <http://dx.doi.org/10.1016/j.compstruct.2013.09.017>



deformation and loading, as well as reduced fabric creasing. The avoidance of sharp corners within the exposed area of the fabric also reduces the possibility of fabric tearing, as observed for the corner plate clamped fabric. It is preferable to use simple shapes for the exposed fabric area. Otherwise, as shown for the corner plate clamped fabric, different regions of the exposed fabric will be subjected to drastically different levels of deformation and loading. Thus, with complex exposed fabric shapes, it becomes difficult to standardize or normalize impact performance, given the many combinations of possible fabric dimensions and designs.

Generally, the greater the extent of free edges in a fabric, the greater the occurrence of yarn pullout. However, for yarn pullout to be a significant source of energy dissipation, at least two sides of the fabric or sufficient areas at the four corners must be clamped to generate sufficient inter-yarn normal contact forces, which in turn results in greater force required to pull the yarns out of fabric weave. Otherwise, as shown for the corner point clamped fabric, while significant extents of both warp and fill yarn pullout occurred, it did not result in significant energy dissipation.

In this study, only a 0–90° fabric orientation was considered, although fabrics can also be clamped in a  $\pm 45^\circ$  orientation which would result in different ballistic impact performance, especially for partially clamped fabric configurations. The fabric orientation makes no difference in a circular clamp because of its symmetry about the vertical axis, while a 4-sided clamp with a 0–90° orientation is the same as a diamond clamp with a  $\pm 45^\circ$  orientation, and vice versa for a square exposed fabric shape. Note that when orienting the fabric in a  $\pm 45^\circ$  orientation for a 2-sided clamp, a rectangular exposed shape results in a combination of yarns that are clamped only at one end and

Please cite this article as: Nilakantan G, Nutt S. *Effects of clamping design on the ballistic impact response of soft body armor*. Composite Structures 108 (2014) 137–150. DOI: <http://dx.doi.org/10.1016/j.compstruct.2013.09.017>



yarns that are free at both ends. However, a square exposed shape results in the central-most yarns being clamped at both ends, while the remaining yarns are free at both ends. These have different effects on the  $V_{50}$  velocities, and thus the dimensions and size of the fabric target is another important consideration. Similarly, the size of the projectile relative to the yarn width and span, as well as the extra length of yarn available due to de-crimping (which is related to the in-plane fabric dimensions) are further considerations that could affect the fabric failure modes (e.g., by promoting a windowing mechanism instead of principal yarn failure). These and other considerations are being systematically addressed, and future studies will build upon the complexity of the model by including multi-layer fabric targets.

**Acknowledgements:** Computation for the work described in this paper was supported by the University of Southern California Center for High-Performance Computing and Communications (hpcc.usc.edu). GN and SN acknowledge support from the M.C. Gill Composites Center.

## **References:**

1. Tabiei A, Nilakantan G. *Ballistic impact of dry woven fabric composites: a review*. Appl Mech Rev 2008;**61**:010801–13.
2. David NV, Gao XL, Zheng JQ. *Ballistic resistant body armor: contemporary and prospective materials and related protection mechanisms*. Appl Mech Rev 2009;**62**:1–20.
3. Cavallaro P. *Soft body armor: an overview of materials, manufacturing, testing, and ballistic impact dynamics*. NUWC-NPT Technical Report 12,057, 2011.
4. Cheeseman BA, Bogetti TA. *Ballistic impact into fabric and compliant composite laminates*. Compos Struct 2003;**61**:161–73.
5. Yang HH. Kevlar aramid fiber. New York: John Wiley & Sons; 1993. p. 71–102.
6. Nilakantan G, Gillespie Jr JW. *Ballistic impact modeling of woven fabrics considering yarn strength, friction, projectile impact location, and fabric boundary condition effects*. Compos Struct 2012;**94**:3624–34.
7. Nilakantan G, Keefe M, Wetzel ED, Bogetti TA, Gillespie Jr JW. *Computational modeling of the probabilistic impact response of flexible fabrics*. Compos Struct 2011;**93**:3163–74.
8. Nilakantan G, Keefe M, Wetzel ED, Bogetti TA, Gillespie Jr JW. *Effect of statistical yarn tensile strength on the probabilistic impact response of woven fabrics*. Compos Sci Technol 2012;**72**:320–9.

Please cite this article as: Nilakantan G, Nutt S. *Effects of clamping design on the ballistic impact response of soft body armor*. Composite Structures 108 (2014) 137–150. DOI: <http://dx.doi.org/10.1016/j.compstruct.2013.09.017>



9. Nilakantan G, Abu-Obaid A, Keefe M, Gillespie Jr JW. *Experimental evaluation and statistical characterization of the strength and strain energy density distribution of Kevlar KM2 yarns: exploring length-scale and weaving effects*. J Compos Mater 2011;**45**:1749–69.
10. Nilakantan G. *Filament-level modeling of Kevlar KM2 yarns for ballistic impact studies*. Compos Struct 2013;**104**:1–13.
11. Nilakantan G, Wetzel ED, Bogetti TA, Gillespie Jr JW. *Finite element analysis of projectile size and shape effects on the probabilistic penetration response of high strength fabrics*. Compos Struct 2012;**94**:1846–54.
12. Nilakantan G, Gillespie Jr JW. *Yarn pull-out behavior of plain woven Kevlar fabrics: effect of yarn sizing, pull-out rate, and fabric pre-tension*. Compos Struct 2013;**101**:215–24.
13. Nilakantan G, Keefe M, Bogetti TA, Gillespie Jr JW. *Multiscale modeling of the impact of textile fabrics based on hybrid element analysis*. Int J Impact Eng 2010;**37**:1056–71.
14. Nilakantan G, Keefe M, Bogetti TA, Adkinson A, Gillespie Jr JW. *On the finite element analysis of woven fabric impact using multiscale modeling techniques*. Int J Solids Struct 2010;**47**:2300–15.
15. Nilakantan G, Wetzel ED, Merrill R, Bogetti TA, Adkinson R, Keefe M, et al. *Experimental and numerical testing of the V50 impact response of flexible fabrics: addressing the effects of fabric boundary slippage*. In: 11<sup>th</sup> International LS-DYNA users conference, MI, USA: Dearborn; June 6–8, 2010.
16. Nilakantan G. *Modeling the impact of flexible textile composites through multiscale and probabilistic methods*. PhD dissertation. Department of materials science and engineering, Newark, DE, USA: University of Delaware; 2010.
17. Chocron S, Figueroa E, King N, Kirchdoerfer T, Nicholls AE, Sagebiel E, et al. *Modeling and validation of full fabric targets under ballistic impact*. Compos Sci Technol 2010;**70**:2012–22.
18. Yu JH, Dehmer PG, Yen CF. *High-speed photogrammetric analysis on the ballistic behavior of Kevlar fabrics impacted by various projectiles*. Army Research Laboratory, Report ARL-TR-5333, September 2010.
19. Song B, Park H, Lu W, Chen W. *Transverse impact response of linear elastic ballistic fiber yarn*. J Appl Mech 2011;**78**:0510231–39.
20. Yu JH, McWilliams B, Dehmer PG, Yen CF. *Experimental measurement and computational simulation of the strains on a single yarn in a Kevlar fabric during stretching*. Army Research Laboratory, Report ARL-TR-5224, 2010.
21. Nilakantan G. DYNAFAB User Manual Version 1.0, Nilakantan Composites. ISBN 978-81-910696-0-0, May 2010.
22. Livermore Software Technology Corporation. LS-DYNA Keyword User's Manual Version 971, May 2007.

Please cite this article as: Nilakantan G, Nutt S. *Effects of clamping design on the ballistic impact response of soft body armor*. Composite Structures 108 (2014) 137–150. DOI: <http://dx.doi.org/10.1016/j.compstruct.2013.09.017>